

Article

Low-Temperature Magnesium Calcium Phosphate Ceramics with Adjustable Resorption Rate

Yulia Lukina ^{1,2,*}, Sergey Kotov ³, Leonid Bionyshev-Abramov ¹, Natalya Serejnikova ^{1,4}, Rostislav Chelmodeev ^{1,5}, Roman Fadeev ^{6,7}, Otabek Toshev ⁸, Alexander Tavtorkin ⁹, Maria Ryndyk ⁹, Dmitriy Smolentsev ¹, Nikolay Gavryushenko ¹ and Sergey Sivkov ¹⁰

¹ National Medical Research Center for Traumatology and Orthopedics named after N.N. Priorov, Ministry of Health of the Russian Federation, Ul. Priorova 10, 127299 Moscow, Russia

² Faculty of Digital Technologies and Chemical Engineering, Mendeleev University of Chemical Technology of Russia, Miusskaya Pl. 9, 125047 Moscow, Russia

³ Building Materials Physico-Chemical Testing Department of the Experimental Tests Preparation and Carry Out Department No. 29, Research Institute of Concrete and Reinforced Concrete (NII ZNB) named after A.A. Gvozdev, JSC Research Center of Construction, Ul. 2 Institutskaya 6, 109428 Moscow, Russia

⁴ Institute for Regenerative Medicine, Sechenov First Moscow State Medical University, Ul. Trubetskaya 8, 119991 Moscow, Russia

⁵ Power Engineering Department, Bauman Moscow State Technical University, Ul. 2 Baumanskaya 5, b.1, 105005 Moscow, Russia

⁶ The Laboratory of Pharmacological Regulation of Cell Resistance, Institute of Theoretical and Experimental Biophysics, Russian Academy of Sciences, 142290 Pushchino, Moscow Region, Russia

⁷ Pushchino State Institute of Natural Science, 142290 Pushchino, Moscow Region, Russia

⁸ Department of Materials Science, Lomonosov Moscow State University, Leninskie Gory 1, 119991 Moscow, Russia

⁹ A.V. Topchiev Institute of Petrochemical Synthesis, Russian Academy of Sciences, Leninskii Pr. 29, 119991 Moscow, Russia

¹⁰ Faculty of Technology of Inorganic Substances and High-Temperature Materials, Mendeleev University of Chemical Technology of Russia, Miusskaya Pl. 9, 125047 Moscow, Russia

* Correspondence: lukina_rctu@mail.ru



Citation: Lukina, Y.; Kotov, S.; Bionyshev-Abramov, L.; Serejnikova, N.; Chelmodeev, R.; Fadeev, R.; Toshev, O.; Tavtorkin, A.; Ryndyk, M.; Smolentsev, D.; et al. Low-Temperature Magnesium Calcium Phosphate Ceramics with Adjustable Resorption Rate. *Ceramics* **2023**, *6*, 168–194. <https://doi.org/10.3390/ceramics6010011>

Academic Editor: Gilbert Fantozzi

Received: 31 October 2022

Revised: 11 December 2022

Accepted: 4 January 2023

Published: 10 January 2023



Copyright: © 2023 by the authors. Licensee MDPI, Basel, Switzerland. This article is an open access article distributed under the terms and conditions of the Creative Commons Attribution (CC BY) license (<https://creativecommons.org/licenses/by/4.0/>).

Abstract: Low-temperature ceramics based on magnesium calcium phosphate cement are a promising resorbable material for bone tissue restoration with the possibility of functionalization. The replacement of the magnesium Mg^{2+} ion with a calcium Ca^{2+} ion at the stage of preparation of the precursor leads to the production of multiphase ceramics containing phases of brushite, monetite, and newberyite, with different dissolution rates. Multiphase ceramics leads to volumetric resorption with preservation of their geometric shape, which was confirmed by the results of an evaluation of the output of magnesium Mg^{2+} and calcium Ca^{2+} ions into the contact solution of the ceramics and the X-ray density of ceramic samples during subcutaneous implantation. The combined introduction of sodium pyrophosphate decahydrate and citric acid monohydrate as setting inhibitors neutralizes their insignificant negative effect on the physico-chemical properties of ceramics (strength, pH, porosity), determining the optimal composition. In vivo experiments with setting inhibitors in the composition of ceramics showed a different biological response, affecting the rate of resorption on par with magnesium ions. Preliminary data on biocompatibility and solubility determined magnesium-calcium phosphate ceramics containing additives that regulate setting to be a potential material for bone tissue restoration and a vector for further research, including in orthotopic implantation models.

Keywords: brushite; newberyite; low-temperature ceramics; volumetric resorption; solubility; subcutaneous implantation; sodium pyrophosphate; citric acid; biocompatibility

1. Introduction

Calcium phosphates are biocompatible, bioactive, and effective for bone tissue regeneration [1,2]. Low-temperature ceramics based on calcium phosphate cements were

formed according to cement technology by the interaction of the initial components in an aqueous medium due to setting and hardening. The high specific surface area and increased resorption rate compared to matrices obtained by high-temperature treatment make low-temperature ceramics a promising material for bone tissue restoration [3–6].

Brushite cement is one of the main types of bioceramics for the production of low-temperature ceramics. Dicalcium phosphate dihydrate $\text{CaHPO}_4 \cdot 2\text{H}_2\text{O}$ (brushite) is usually obtained by the interaction of tricalcium phosphate (TCP) and monocalcium phosphate monohydrate (MCPM) with the formation of a metastable phase under physiological conditions [7–9]. Due to its metastability, brushite-based ceramics have a high resorption rate and high potential as drug delivery systems (vancomycin, doxycycline, chlorhexidine, trolox), protein growth factors [10–12], and as a material for bone replacement [10,13].

It is known that the presence of the bioactive Mg^{2+} ion in the structure of calcium phosphates plays an essential role in the biological process and stimulates bone formation [14–17]. Magnesium is an obligate cofactor of alkaline phosphatase and many enzymatic reactions, which participates in the synthesis of bone collagen in cell proliferation and differentiation, cell–matrix interaction, and the normal functioning of organs [18–21].

One of the important features of the presence of the magnesium ion Mg^{2+} in the composition of brushite when replacing the calcium ion Ca^{2+} is the stabilization of the phase composition [20–24]. Magnesium ions inhibit the formation of less soluble calcium phosphates (hydroxyapatite, tricalcium phosphate, octacalcium phosphate) in vivo in brushite materials [24–30], since magnesium acts as a strong inhibitor of crystal growth in less soluble calcium phosphates. In this regard, magnesium calcium phosphate ceramics do not recrystallize over time, unlike brushite, during a long-term in vivo experiment. The high rate of resorption is maintained [21,31].

The formation of an additional phase of dimagnesium phosphate $\text{MgHPO}_4 \cdot 3\text{H}_2\text{O}$ trihydrate (newberyite) in addition to the main phase of brushite $\text{CaHPO}_4 \cdot 2\text{H}_2\text{O}$ can increase the rate of resorption. When high concentrations of Mg^{2+} ions were introduced into the composition of brushite cement, newberyite was formed. Its solubility is at 25 °C- $\log(\text{Ksp})$ is 5.51–5.82, whereas the solubility of brushite- $\log(\text{Ksp}) = 6.59$ [7,16,17,23,32,33].

Volumetric resorption of newberyite and superficial resorption of brushite were observed by Klammert et al. using a model of subcutaneous implantation in rats [17].

We assumed that the advantage of a two-phase product of a controlled composition may be a different rate of volumetric dissolution of the phases with the preservation of the geometric shape of the matrix, followed by its germination by newly formed bone tissue and gradual complete resorption of the matrix.

Brushite cement has a very short setting time, as is known. Despite the fact that rheological properties are not crucial for the production of ceramic matrices using cement technology, the setting time should be sufficient to form scaffolds of the required geometry. Additives of substances containing $\text{P}_2\text{O}_7^{4-}$ pyrophosphate- and $\text{C}_6\text{H}_5\text{O}_7^{3-}$ citrate-ions are the most common and effective regulators of the setting of brushite cements [34–37]. After adsorption, these ions form poorly soluble compounds on the particles of the initial components and reduce the electrostatic attraction. The reaction is slowed down. It is also known that when calcium ions are replaced with magnesium in TCP-based brushite cements, the setting time increases, and the mechanical properties of calcium phosphates improve [33].

However, none of the abovementioned reports have focused on the study of the effect of Mg substitutions in TCP, leading to the production of ceramics based on brushite-newberyite cement containing set-retarding additives, on the properties of ceramics, including solubility and biocompatibility.

Therefore, the main purpose of this study was to investigate the effect of Mg substitutions in TCP in the production of magnesium calcium phosphate ceramics based on brushite-newberyite cement containing set-retarding additives.

2. Materials and Methods

$Mg_xCa_{(3-x)}(PO_4)_2$ was obtained during solid-phase synthesis of a homogeneous mixture of the precursors $CaHPO_4$, $CaCO_3$, $Mg_2P_2O_7$, and $Mg(OH)_2$ in accordance with Table 1 at a temperature of 1100 °C for 6.5 h. The sintered material was crushed in a planetary ball mill for 20 min in an acetone medium with zirconium oxide balls with a diameter of 10 mm at a ratio of powder weight/ball weight = 1/3. The powder was dried at a temperature of 50 °C.

Table 1. Precursor ratios for $Mg_xCa_{(3-x)}(PO_4)_2$ production.

| C_{OCTaB} | Amount of Precursor, mol | | | |
|-------------|--------------------------|----------|--------------|------------|
| | $CaHPO_4$ | $CaCO_3$ | $Mg_2P_2O_7$ | $Mg(OH)_2$ |
| Mg0 | 2 | 1 | 0 | 0 |
| Mg0.75 | 3 | 1.5 | 0.5 | 0.5 |
| Mg1.5 | 1 | 0.5 | 0.5 | 0.5 |
| Mg2.25 | 1 | 0.5 | 1.5 | 1.5 |

Magnesium-calcium phosphate ceramics were obtained during acid–base interaction by mixing synthesized $Mg_xCa_{(3-x)}(PO_4)_2$ ($x = 0–2.25$ —compositions Mg0, Mg0.75, Mg1.5, Mg2.25) and monocalcium phosphate monohydrate $Ca(H_2PO_4)_2 \cdot H_2O$ with liquid content in a ratio of 55/45. The mixing liquid was distilled water or a solution of sodium pyrophosphate hexahydrate (SPP) salt or a solution of citric acid monohydrate (CA). The liquid/powder ratio was (L/P) 0.6 or 0.7.

The mechanical compressive strength of the matrices was determined on samples using cylinders with a diameter of 10 mm and a height of 10 mm by means of the universal testing machine LFV 10–50 T (Walter + Bai AG, Switzerland) at a loading speed of 8 mm/min on the 1st day after molding. Samples were stored in a 100% humidity box at 37 °C and dried. The results of the compressive strength test were expressed as the mean \pm standard error of the mean of fivefold determinations.

The setting time of the cement pastes was determined using a small Vicat needle technique. Half a minute after placing the pastes into a metallic ring with a height of 9 mm, the indenter (136 g mass, 1 mm diameter of the needle) was lowered vertically onto the surface of the cement. The indentation was repeated at intervals of 5 s. The time at needle penetrations of 1 mm was taken as the initial setting time. The time at needle penetrations of 9 mm was taken as the finishing time. The results of the determination of the setting time are the average value of the threefold definitions.

The pH of the medium in contact with the materials was determined using the laboratory pH meter Seven Compact S210 (Mettler-Toledo GmbH, Greifensee, Switzerland). The ratio of the weight of the sample granules with a diameter of 4 mm and a height of 2 mm to the mass of distilled water was 1:10. The pH of the contact medium was measured after 10 min while keeping samples in distilled water. The results of the pH determination were recorded as the mean value \pm standard error of the mean value of the fivefold definitions.

The granulometric composition was studied using the particle size and shape analyzer CAMSIZER[®] X2 (MICROTRAC RETSCH GmbH, Haan, Germany). The results of the determination of the particle size and surface area were expressed as the average value \pm standard error of the average value of threefold definitions.

The porosity was determined on samples using cylinders with a diameter of 10 mm and a height of 10 mm by hydrostatic weighing in an inert liquid (kerosene) on the 1st day after molding. Samples were stored in a 100% humidity box at 37 °C and dried. The results of the porosity determination were expressed as the average value \pm standard error of the average value of the fivefold definitions.

X-ray powder diffraction (XRD) analysis used an ARL Equinox 1000 X-ray diffractometer (Thermo Fisher Scientific INEL SAS, Saint-Herblain, France). The survey was carried out in the reflection mode using CuK α radiation (angle interval 2θ : from 5° to 45° or 68°,

step 2θ 0.03°). In the qualitative analysis of the resultant X-ray diffraction patterns, we used WinXPOW software and the ICDD PDF-2 database.

In the quantitative analysis, we used the reference intensity ratio method (with the I/I_c intensity ratio of the strongest lines of the substance and corundum ($\alpha\text{-Al}_2\text{O}_3$) in a mixture containing 50 wt. % of both components). (Chung method) [38]. The weight fraction was calculated using the relation

$$\omega_A = \frac{I_{iA} / (I/I_c(A)) \cdot I_{iA}^{rel}}{\sum I_{iK} / (I/I_c(K)) \cdot I_{iK}^{rel}}$$

where I_{iA} is the measured intensity of the i th reflection from phase A; I_{iA}^{rel} is the relative intensity of this reflection in the database; $I/I_c(A)$ is the corundum number for the phase A being determined; and I_{iK} , I_{iK}^{rel} , and $I/I_c(K)$ are the corresponding quantities for all components of the mixture (including A). The calculation was carried out on characteristic lines, on which the lines of other phases were not superimposed. XRD measurements for all the investigated compositions were repeated two or three times in two or three independent samples. The results of the XRD determination were expressed as the average value \pm standard error of the average value of the threefold definitions in in vitro experiments and of the twofold definitions in in vivo experiments.

The microstructure was studied using a scanning electron microscope Phenom XL G2 (Thermo Fisher Scientific, Breda, Netherlands). The accelerating voltage was 15 kV. Silver was sprayed with the magnetron sprayer Cressington 108auto (Cressington Scientific Instruments Ltd., Watford, UK).

Elemental analysis was carried out by means of a special detector (energy dispersion spectrometer); data analysis was carried out in the INCA—Point & ID program. The results of EDS determination were expressed as the value of the onefold definition.

The solubility of ceramics samples with a diameter of 4 mm and a height of 2 mm was evaluated by measuring the concentration of calcium and magnesium ions in saline solution. The ratio of granules to liquid was 1/10 mL. Samples were kept in a shaker incubator IKA KS 3000 (IKA[®]-Werke GmbH & Co. KG, Staufen, Germany) at 37 °C for 5 days. When choosing an aliquot, it was replaced with a fresh solution. The concentration of calcium and magnesium ions in the solution was determined on a PE540054005400 HA spectrophotometer (Ekros-Analytics LLC, Saint Petersburg, Russia) at a wavelength of 570 nm and 540 nm, respectively, during the formation of colored complexes of calcium ions with o-cresolphthalein complexone and of magnesium ions with xylydine blue. The results of the determination of the concentrations of calcium and magnesium in the solution were expressed as the average value \pm standard error of the average value of threefold definitions.

Statistical analysis. The data were recorded as average \pm standard error and analyzed using the Origin Pro 2021 software. One-way ANOVA tests ($p < 0.05$) were used to determine the significance of the differences between the groups. Significant differences ($p < 0.05$) between different materials at one time point are labeled with *.

A cell viability test was carried out on samples of magnesium calcium phosphate matrixes with a diameter of 4 mm and a height of 2 mm. Mesenchymal stromal cells of human bone marrow were used. The cells were cultured in alfa MEM (Sigma-Aldrich, St. Louis, MO, USA) with the addition of 10% embryonic calf serum (Gibco, Carlsbad, CA, USA) and 40 mcg/mL gentamicin sulfate (Sigma-Aldrich, USA), at 37 °C, under conditions of 5% CO₂ content in the air. Cultured cells of 1–4 passages were used in the experiments. Subcultivation of the cells was carried out in alfa MEM medium with 10% embryonic calf serum and 40 mcg/mL of gentamicin sulfate, at 37 °C, under conditions of 5% CO₂ content in the air. The number of living and dead cells was determined by staining cells with fluorescent dyes calcein AM (Sigma-Aldrich, St. Louis, MO, USA) and propidium iodide (Sigma-Aldrich, St. Louis, MO, USA). The cells were detached from the surface of the samples using an Accutase cocktail. Cells were stained in L-15 medium with 1% embryonic

calf serum containing 1 mcg/mL of calcein AM and 2 mcg/mL of propidium iodide for 25 min at 37 °C. The analysis of living and dead cells was carried out using an Accuri C6 flow cytometer (BD Bioscience, San Jose, CA, USA). The results of the experiments were presented as an average \pm standard error.

The study of the biological response of magnesium calcium phosphate matrixes was carried out with a Wistar rat model (a subcutaneous implantation into the hypodermis of male rats with a mass of \approx 250–300 g). The total number of animals was 15. The animals were divided into three groups of 5. The animals in the first group were implanted with ceramic samples N0, N20, N40, and N60 containing PPS. Animals of the second group were implanted with ceramic samples N0, N20, N40, and N60 containing CA. Animals of the third group were implanted with ceramic samples N0, N20, N40, and N60 containing CA_PPS. The surgical interventions were fulfilled under intramuscular anesthesia with Zoletil (7 mg/kg) and Xylazine (13 mg/kg). The procedure was performed under aseptic conditions. Before the treatment, the surgical field was shaved and sanitized with an antiseptic. The animal was placed on its stomach. An incision was made along the spine. In the hypodermis, 4 caverns were formed by pushing the tissues apart. The samples were implanted in these caverns. The implantation period was 11 weeks. All surgical procedures and conditions of keeping animals complied with the ethical rules for experiments with animals, including the European Directive FELASA-2010. Tomographic examination was performed in vivo after surgery and then weekly after implantation.

For morphological study, samples of connective tissue capsules were fixed in neutral buffered formalin (10%), dehydrated, and paraffin embedded. Sections (with a thickness of 4 μ m) were prepared and stained with hematoxylin-eosin. They were studied with a Leica DM 4000 B LED (Leica Microsystems Wetzlar GmbH, Wetzlar, Germany) microscope with a Leica DFC 7000 T camera under standard light and phase-contrast visualization modes. A maturity of scar tissues around the samples was evaluated with its thickness and a relative area of blood vessels. The high maturity corresponds to a minimal inflammation in the low-thickness tissues with a small amount of the vessels. In the ImageJ program, the thickness of the capsules (at 50 \times magnification) and the relative area of the vessels (at 200 \times magnification) were measured from microphotographs of histological sections. Statistical analysis of the results was performed using an unpaired Student's t-test and one-way ANOVA test followed by Tukey's comparison test. The results were considered reliable at $p \leq 0.05$. The procedure was carried out with GraphPad Prism 7.00. The results were presented in terms of the mean \pm standard error.

Micro-CT of the samples was performed on an X-ray microtomograph Bruker SkyScan 1178 (BRUKER BELGIUM, Kontich, Belgium) at a voltage of 65 Kv and a current of 615 Ma, with an Al 0.5 mm filter. The spatial resolution was 84 microns/pixel. The reconstruction of the slices was carried out with NRecon v.1.6.10.4 software, and densitometric measurements were made in the CTAn v.1.20.3.0 program. The data were recorded as the average \pm standard error and analyzed using Origin Pro 2021 software. One-way ANOVA tests ($p < 0.05$) were used to determine the significance of the differences between the groups. Significant differences ($p < 0.05$) between different materials at one time point were labeled with *, and significant differences at a specific time point between different groups were labeled with #, @, and &.

3. Results

3.1. Synthesis of $Mg_xCa_{(3-x)}(PO_4)_2$ Powders for the Production of Ceramics N0, N20, N40, N60

The amount of magnesium (x) in the composition of $Mg_xCa_{(3-x)}(PO_4)_2$ was chosen so that in ceramics, the ratio of phases $MgHPO_4 \cdot 3H_2O$ (newberyite) and $CaHPO_4 \cdot 2H_2O$ (brushite) was 0/100 (composition N0), 20/80 (composition N20), 40/60 (composition N40), and 60/40 (composition N60) with a ratio of the initial cement components of 55/45. The calculated amount of magnesium in $Mg_xCa_{(3-x)}(PO_4)_2$ was Mg0 (for N0), Mg0.75 (for N20), Mg1.5 (for N40), and Mg2.25 (for N60).

The products of solid-phase synthesis are magnesium-calcium phosphates of variable composition with the general formula $Mg_xCa_{(3-x)}(PO_4)_2$ c \times 0 (Mg0), \times 0.75 (Mg0.75),

$\times 1.5$ (Mg1.5), $\times 2.25$ (Mg2.25). Figure 1 shows diffractograms of magnesium calcium phosphate powders. The $\text{Mg}_x\text{Ca}_{(3-x)}(\text{PO}_4)_2$ Mg1.5 diffractogram corresponds to magnesium calcium phosphate $\text{Mg}_3\text{Ca}_3(\text{PO}_4)_4$ (73-1182 PDF-2). The Mg0.75 diffractogram contains peaks characteristic of tricalcium phosphate $\text{Ca}_3(\text{PO}_4)_2$ (70-2064 PDF-2) and peaks characteristic of $\text{Mg}_3\text{Ca}_3(\text{PO}_4)_4$. Along with the peaks of $\text{Mg}_3\text{Ca}_3(\text{PO}_4)_4$, the diffraction pattern $\text{Mg}_x\text{Ca}_{(3-x)}(\text{PO}_4)_2$ Mg2.25 contains peaks characteristic of trimagnesium phosphate $\text{Mg}_3(\text{PO}_4)_2$ (75-1491 PDF-2).

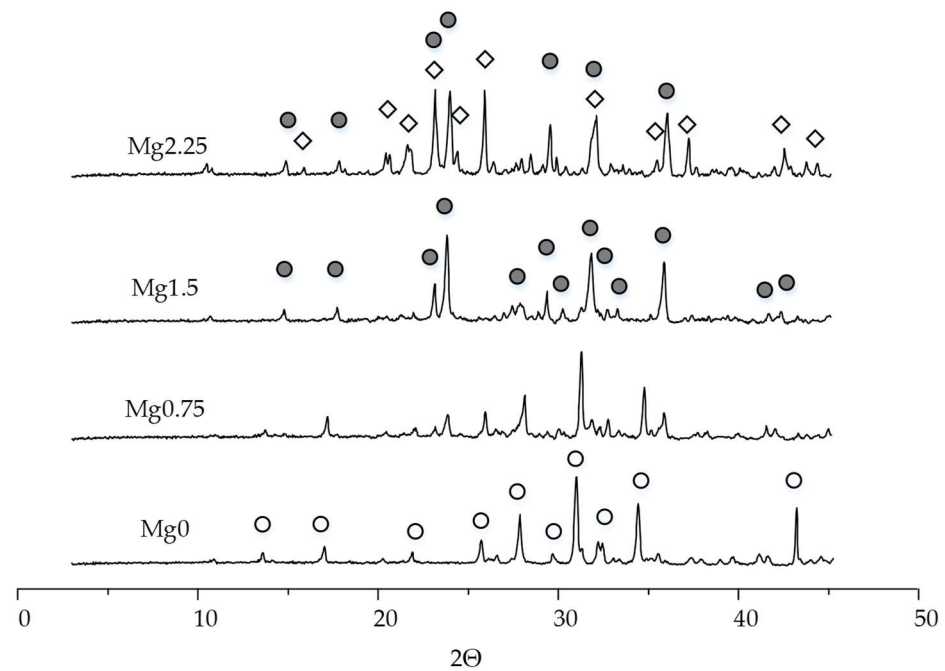


Figure 1. X-ray diffraction pattern of $\text{Mg}_x\text{Ca}_{3-x}(\text{PO}_4)_2$ powders for Mg0, Mg0.75, Mg1.5, Mg2.25, where \circ is tricalcium phosphate $\text{Ca}_3(\text{PO}_4)_2$ (TCP); \bullet is magnesium calcium phosphate $\text{Mg}_3\text{Ca}_3(\text{PO}_4)_4$; and \diamond is trimagnesium phosphate $\text{Mg}_3(\text{PO}_4)_2$.

The parameters of the granulometric composition are presented in Table 2. Comparison is not statistically significant at $p > 0.05$, and the average particle size of the obtained powders was 6.2–6.8 microns.

Table 2. Surface area and average particle size of $\text{Mg}_x\text{Ca}_{3-x}(\text{PO}_4)_2$ powders for Mg0, Mg0.75, Mg1.5, and Mg2.25.

| Parameter | Mg0 | Mg0.75 | Mg1.5 | Mg2.25 |
|--------------------------------------|---------------------|---------------------|---------------------|---------------------|
| Surface area, m^2/g | 3.4399 ± 0.0741 | 3.2795 ± 0.1916 | 3.4947 ± 0.1083 | 3.6986 ± 0.1854 |
| Average particle size, μm | 6.69 ± 0.23 | 6.80 ± 0.20 | 6.57 ± 0.21 | 6.20 ± 0.20 |

The particles of all compositions had an irregular shape. The particle size did not differ for all compositions (Figure 2). The results of energy dispersion analysis confirm the variable composition of the solid-phase synthesis product (Table 3). Mg/Ca ratios determined by EDS resulted in Mg0.75, Mg1.5, and Mg2.25 composition of 0.74/2.26, 1.51/1.49, and 2.17/0.83, respectively. This is slightly different from the target values.

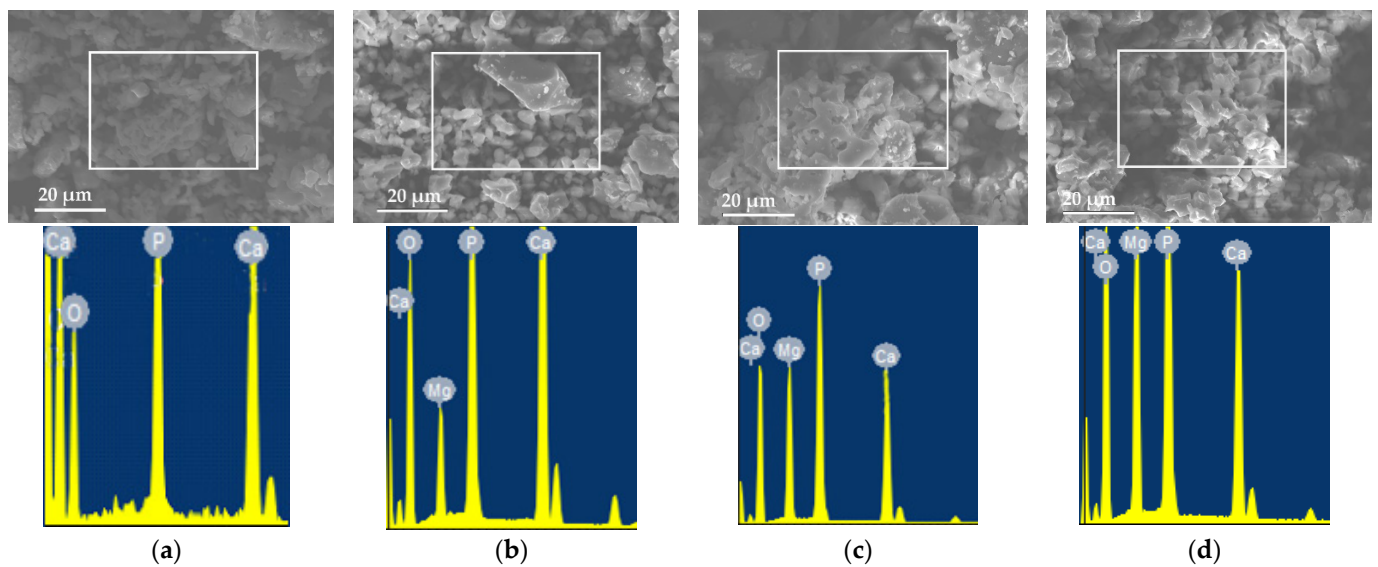


Figure 2. Micrographs and corresponding tested area and EDS spectra of $Mg_xCa_{3-x}(PO_4)_2$ powders for the production of ceramics compositions: (a) Mg0; (b) Mg0.75; (c) Mg1.5; (d) Mg2.25. Magnification $\times 3000$.

Table 3. EDS results for the selected area of Figure 2.

| Atomic Concentrations, % | Elemental Symbol | | | |
|--------------------------|------------------|------|------|------|
| | O | Mg | P | Ca |
| Mg0 | 71.1 | 0 | 11.9 | 17.7 |
| Mg0.75 | 70.4 | 4.4 | 12.0 | 13.4 |
| Mg1.5 | 69.5 | 9.1 | 12.2 | 9.0 |
| Mg2.25 | 69.5 | 13.5 | 12.8 | 5.2 |

3.2. Cements and Ceramics Characterizations

3.2.1. Setting Times of Cements

The ratio of liquid to powder of 0.6 mL/g was used to obtain cement dough. In order to obtain low-temperature ceramics in the form of blocks or granules, it is necessary to prevent the cement from setting within 3 min.

The initial setting time of additive-free compositions was less than 30 s. Sodium pyrophosphate hexahydrate $Na_4P_2O_7 \cdot 10H_2O$ (SPP) and citric acid monohydrate $C_6H_8O_7 \cdot H_2O$ (CA) were used as retarding additives for the hydration process. The additives were introduced separately and together in the form of solutions with different concentrations. The results of determining the initial and finish setting are presented in Table 4. Acceptable setting times for each cement composition (N0, N20, N40, N60) and the type of additive are highlighted in color.

With an increase in the number of magnesium ions in $Mg_xCa_{3-x}(PO_4)_2$, the setting time increases. To obtain an initial setting no earlier than 3 min, a lower concentration of retarding additives is required. The required concentration of SPP is directly proportional to the amount of $CaHPO_4 \cdot 2H_2O$ in the final composition. In the process of slowing down the reaction, the mechanism of formation of poorly soluble calcium pyrophosphates on the surface of the initial components is probably less important than the mechanism of binding of $P_2O_7^{4-}$ ions to the nuclei of reaction products, embedding these ions into the crystal lattice, which stops growth and aggregation.

Table 4. Setting time of cements based on $Mg_xCa_{3-x}(PO_4)_2$ powders for obtaining ceramics compositions N0, N20, N40, and N60.

| Composition → | N0 | | N20 | | N40 | | N60 | |
|----------------------------|---------|--------|---------|-------|---------|-------|---------|-------|
| Additives ↓ Setting Time → | Initial | Final | Initial | Final | Initial | Final | Initial | Final |
| 0.3 M CA | 5:30 | 3:40 * | | | | | 11:00 | 6:10 |
| 0.295 M CA | | | 5:30 | 3:35 | | | | |
| 0.289 M CA | | | | | 8:00 | 3:40 | | |
| 0.284 M CA | | | | | | | 8:30 | 3:50 |
| 0.066 M SPP | 4:40 | 3:40 | 23:59 | 8:00 | | | | |
| 0.055 M SPP | | | 4:50 | 3:35 | | | | |
| 0.043 M SPP | | | | | 4:45 | 3:30 | | |
| 0.033 M SPP | 2:30 | 2:00 | 3:30 | 2:20 | 4:30 | 2:30 | 5:00 | 3:45 |
| 0.031 M SPP | | | | | | | 4:45 | 3:05 |
| 0.1 M CA + 0.033 M SPP | 3:30 | 3:05 | 6:30 | 3:10 | 19:30 | 12:00 | | |
| 0.05 M CA + 0.033 M SPP | | | | | 5:45 | 3:10 | | |
| 0.05 M CA + 0.015 M SPP | | | | | 2:45 | 2:00 | 5:10 | 3:00 |

* the optimal setting time for each composition is highlighted in color.

3.2.2. Phase Compositions and Microstructures of Ceramics

X-ray phase analysis of ceramics based on $Ca_3(PO_4)_2$ powder, performed after 7 days of hardening of the samples in wet conditions, showed the presence of $CaHPO_4 \cdot 2H_2O$ brushite (72-713 PDF-2) and dihydrophosphate $CaHPO_4$ monetite (70-359 PDF-2) as the main phases (Figure 3), with a significant advantage with monetite. This is due to the high reactivity of $Mg_xCa_{3-x}(PO_4)_2$, high heat generation, and small particle size, which increases water requirements.

The possibility of separate and joint use of the additive inhibitors SPP and CA on the properties of ceramics in experiments in vitro and in vivo with the example of ceramics N0 were investigated in this work. The study of the effect of the concentration of magnesium ions in magnesium-calcium phosphate ceramics was carried out for compositions N0, N20, N40, and N60 at optimal concentrations of a mixture of additives for each composition in accordance with Table 4.

The introduction of retarding additives significantly affects the composition, increasing the amount of brushite in the composition of ceramics. In compositions with 0.3 M CA and 0.1 M CA + 0.033 M SPP, the amount of the $CaHPO_4 \cdot 2H_2O$ phase is higher than when using 0.066 M SPP solution. A combination of retarding additives and an increase in the L/P ratio to 0.7 is necessary to obtain a single-phase brushite product.

When using $Mg_xCa_{3-x}(PO_4)_2$ at Mg0.75, Mg1.5, and Mg2.25, newberyite $MgHPO_4 \cdot 3H_2O$ (72-23 PDF-2) is present in the composition of ceramics N20, N40, and N60 in addition to the phases $CaHPO_4 \cdot 2H_2O$ and $CaHPO_4$ (Figure 4). An increase in the L/P ratio from 0.6 to 0.7 slightly reduces the amount of monetite and does not allow it to be completely excluded. The amount of newberyite, according to the calculation of corundum numbers, has slightly lower values than predicted. The difference increases from N20 to N60.

The microstructure of ceramics is mainly represented by sharp-angled lamellar and prismatic (in the form of parallelepipeds) crystals of brushite and monetite with a length of mainly less than 10 microns (Figure 5). Crystals of up to 20–30 microns in length are observed at the boundary of the pore space, where there are no obstacles to growth. Retarder additives reduce the size of crystals located at the boundaries of pores. When magnesium is introduced into ceramics, prismatic crystals are observed (shown by arrows), similar to newberyite crystals, according to the literature data [32,39,40].

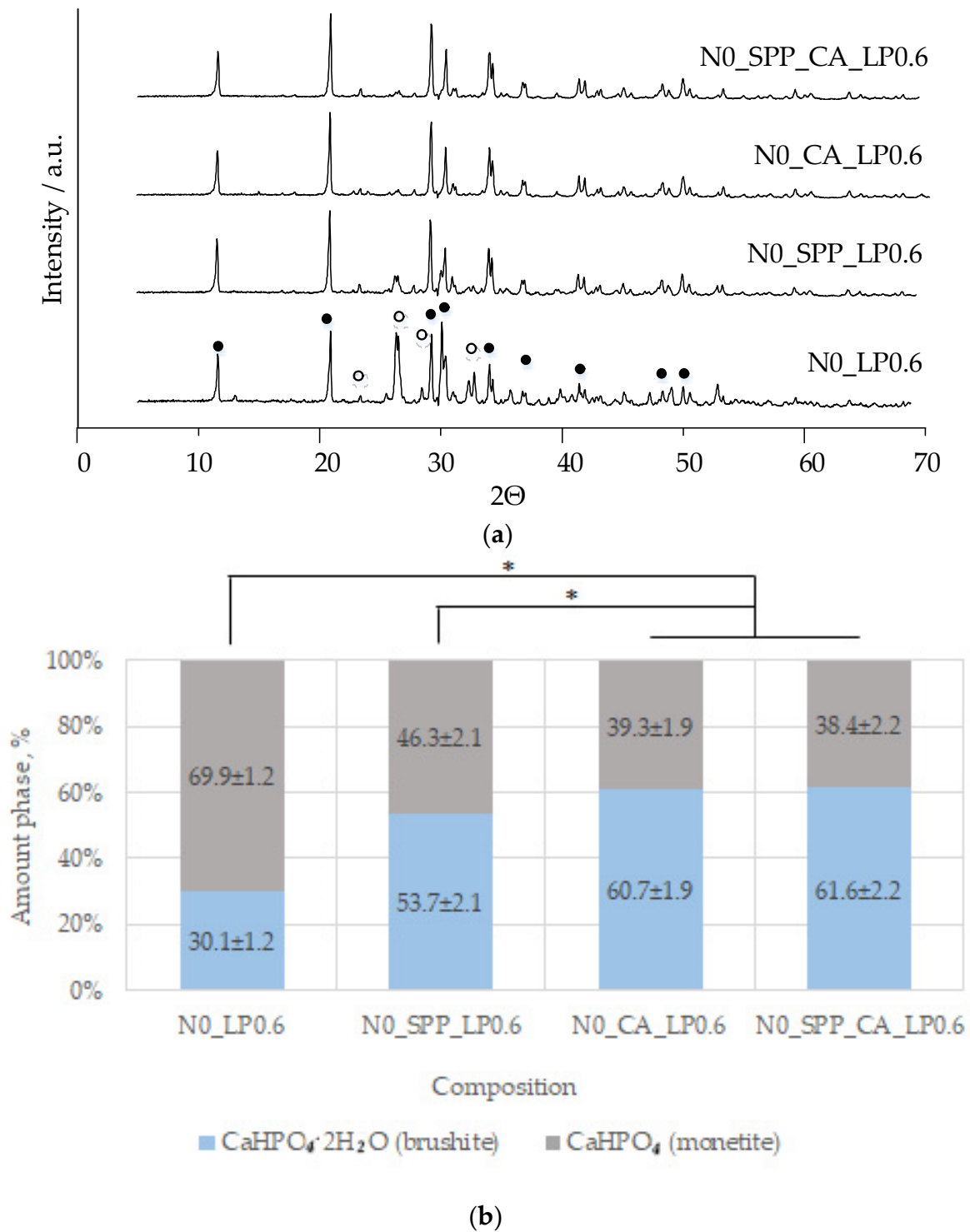


Figure 3. Diffractograms (a) and quantitative phase composition (b) of ceramics: ● CaHPO₄·2H₂O (brushite); ○ CaHPO₄ (monetite). Significant differences are labeled with * ($p < 0.05$).

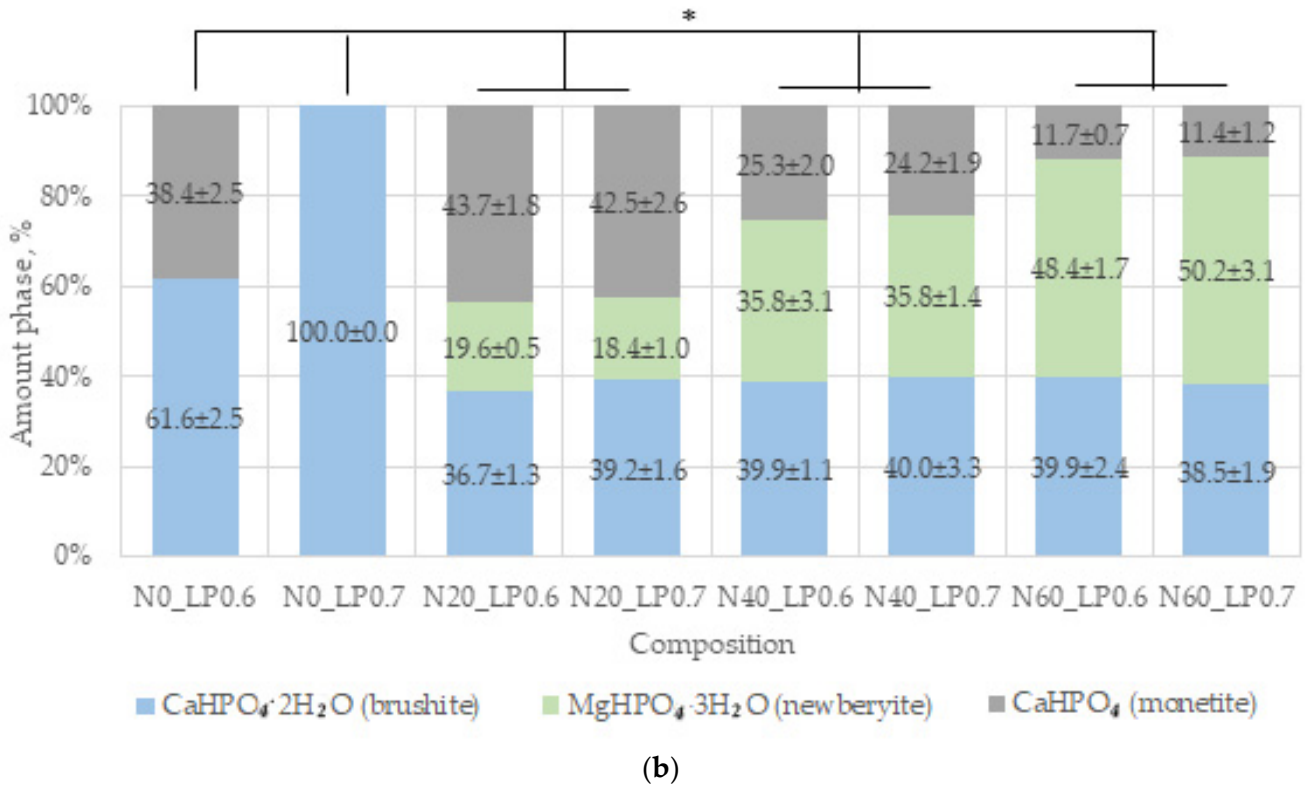
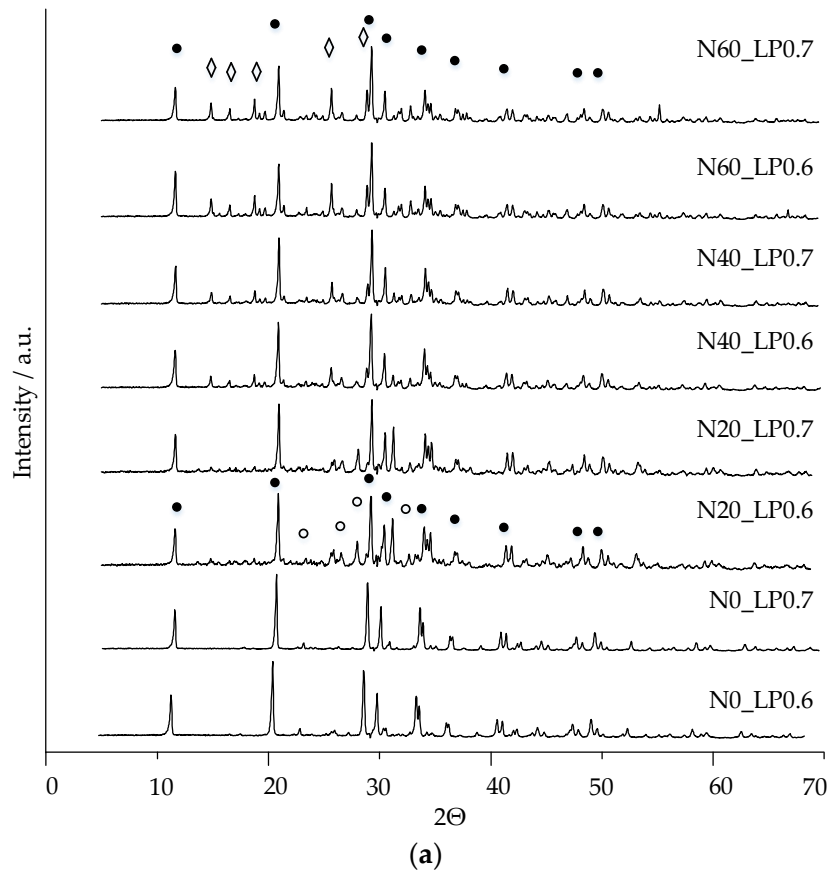


Figure 4. Diffractograms (a) and quantitative phase composition (b) of ceramics with SPP and CA: ● CaHPO₄·2H₂O (brushite); ○ CaHPO₄ (monetite); ◇ MgHPO₄·3H₂O (newberyite). Significant differences are labeled with * (*p* < 0.05).

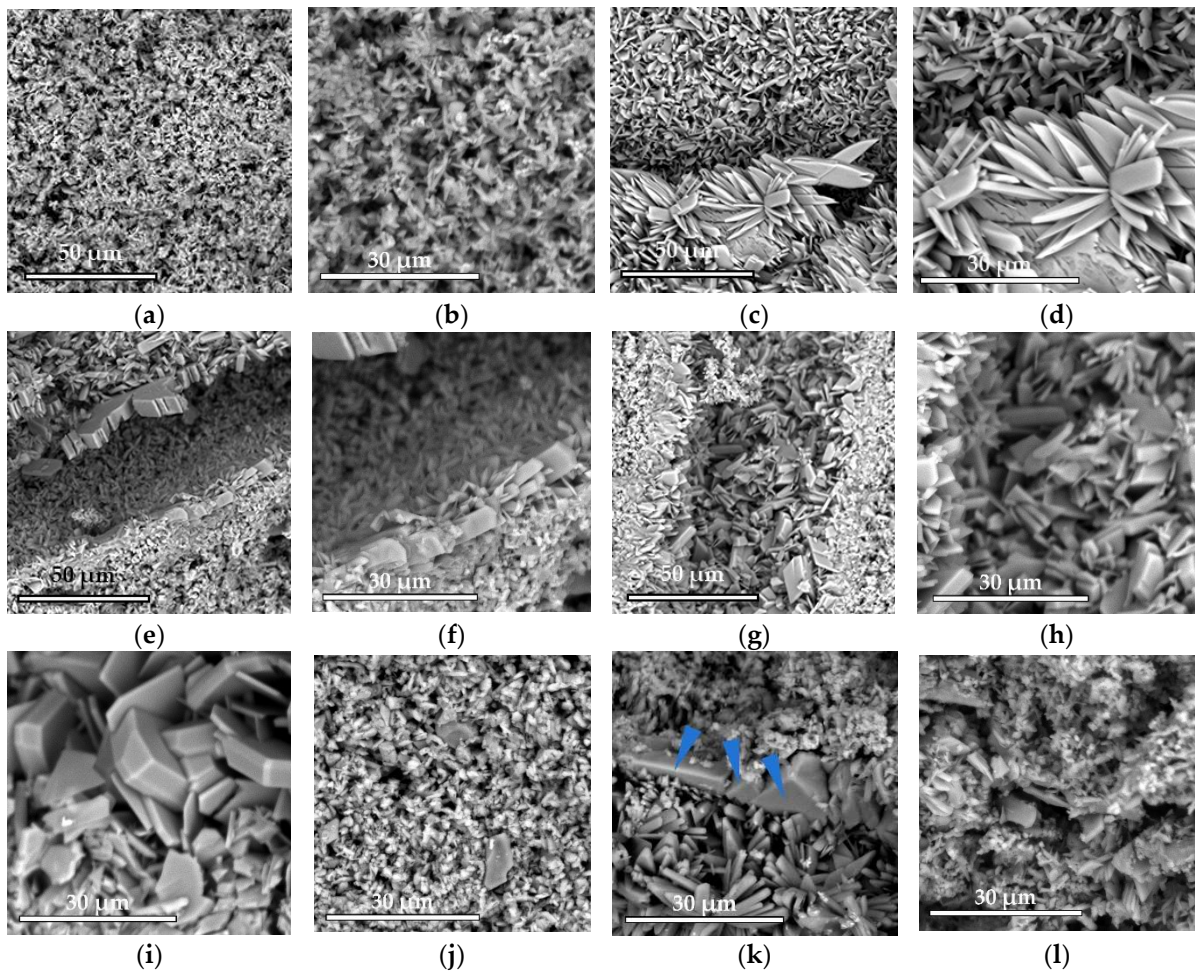


Figure 5. Micrographs of ceramics: N0_LP0.6 (a–d); N0_SPP_LP0.6 (e,f); N0_CA_LP0.6 (g,h); N0_LP0.7 (i); N20_LP0.7 (j); N40_LP0.7 (k); N60_LP0.7 (l). Magnification $\times 2500$ for (a,c,e,g). Magnification $\times 5000$ for (b,d,f,h–l).

3.2.3. Properties of Ceramics

Setting-inhibitor additives slightly reduce the porosity of the ceramics, which we associate with a slight compaction of the structure due to an increase in the setting time and an increase in contacts due to the formation of plate crystals of smaller size. With the introduction of CA, porosity decreases more than with the introduction of a mixture of SPP and CA additives.

The porosity of ceramics decreases with an increase in the amount of magnesium in $Mg_xCa_{3-x}(PO_4)_2$ and, accordingly, newberyite in the final composition of magnesium calcium phosphate ceramics (Figure 6). As expected, porosity increases with an increase from L/P 0.6 to L/P 0.7, which is associated with a decrease in the strength of the coagulation structure and a decrease in cohesion. Porosity values in the range from N0 to N60 do not differ by more than 6.3% at L/P 0.6 and 9.1% at L/P 0.7. The pore size, according to SEM data, is up to 10 μm .

With the introduction of SPP, the mechanical strength of ceramics decreases and increases with the introduction of CA (Figure 6). An increase in the hardening time leads to a longer formation of the microstructure, increasing its density and the number of contacts. The increase in the strength of the ceramics directly depends on the amount of magnesium in the composition of the initial $Mg_xCa_{3-x}(PO_4)_2$. This is due to a decrease in porosity and an increase in the density of the structure. A slight decrease in the strength of N60_SP_CA_LP 0.7 compared to N40_SP_CA_LP 0.7 is within the margin of error and is not significant.

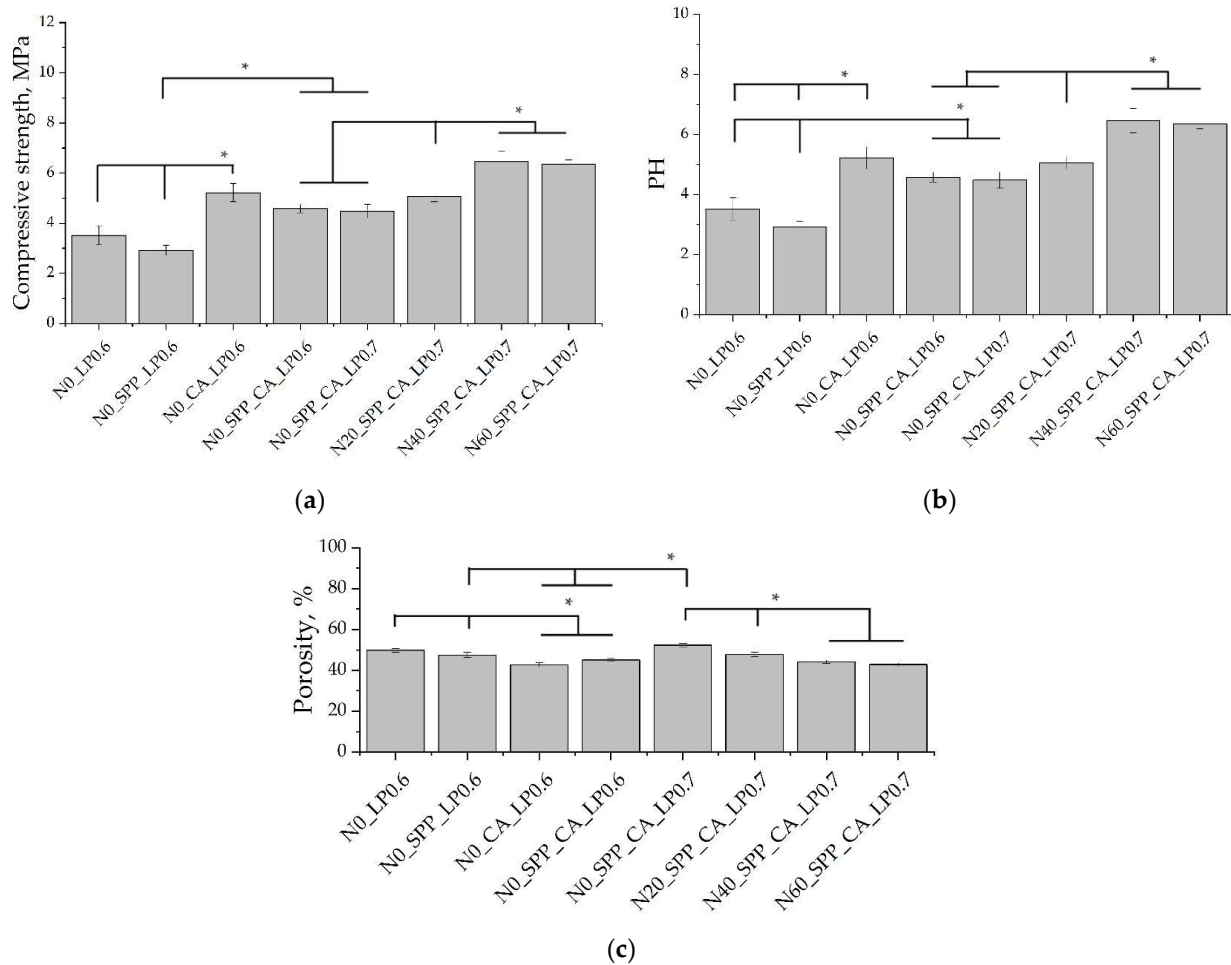


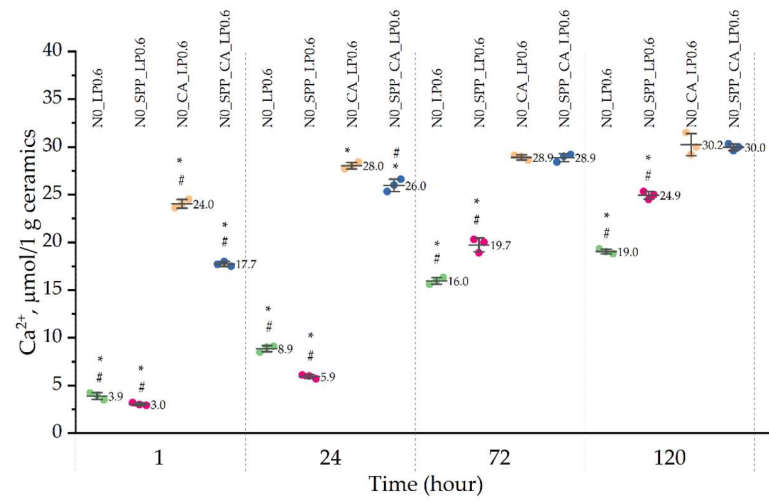
Figure 6. The characteristics of ceramics: (a) compressive strength; (b) pH; (c) porosity. Significant differences are labeled with * ($p < 0.05$).

SPP slightly increases the pH (Figure 6). This is probably due to a slight decrease in the solubility of brushite due to the pyrophosphate shell in the initial periods of interaction with the contact medium. The introduction of CA negatively affects the pH values. This is expected due to its own low pH values and the likely formation of soluble calcium citrates in the ceramic structure. An increase in pH values is observed in the range N0-N20-N40-N60. The combined administration of CA and SPP reduces the negative effect of the CA additive on the pH of ceramics.

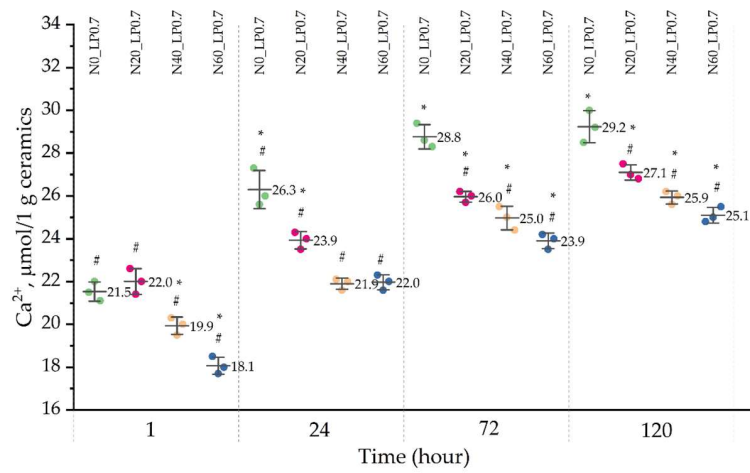
Porosity values in the range from N0 to N60 do not differ by more than 6.3% at L/P 0.6 and 9.1% at L/P 0.7. The pore size, according to SEM data, is up to 10 μm .

3.2.4. Solubility and Phase Compositions, Microstructures of Ceramics after Incubation in Saline Solution

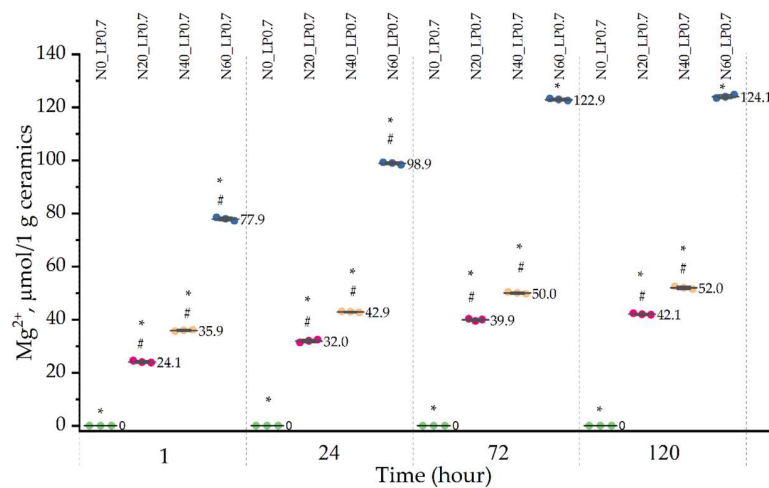
The solubility of ceramics was estimated by the yield of Ca^{2+} and Mg^{2+} ions at a temperature of 37 $^{\circ}\text{C}$ and a rotation speed of 120 rpm in a contact saline solution. The concentration of calcium and magnesium ions in the saline solution after holding ceramics in it is shown in Figure 7.



(a)



(b)



(c)

Figure 7. Behavior of samples of ceramics in saline solution during exposure: change in concentration of Ca²⁺ ions when introducing retarders into the composition: N0 (a), Ca²⁺ ions for N0, N20, N40, 60 (b) and Mg²⁺ ions for N0, N20, N40, N60 (b,c). Significant differences ($p < 0.05$) within one group of materials at consecutive time points are labeled #, and significant differences at a specific time point between different groups are labeled with *.

Set-retarding additives have different effects on the solubility of ceramics and, accordingly, on the yield of calcium ions (Figure 6a). Twenty-four μmol Ca^{2+} was detected after an hour in the contact medium N0_CA_LP0.6, whereas in the contact medium of the composition N0_SPP_LP0.6, such values were reached only after 120 h. An hour after the immersion of N0_SPP_LP0.6 in saline, the concentration of Ca^{2+} was lower than that in the composition N0_LP0.6. The concentration of Ca^{2+} ions in N0_SP_LP0.6 increased significantly after 24 h and exceeded the concentration of Ca^{2+} in N0_LP0.6. Concentrations of Ca^{2+} ions when the two retardant additives SPP and CA (N0_SPP_CA_LP0.6) were introduced simultaneously had an intermediate position: by 1 h, the concentration of Ca^{2+} was 16 μmol , which was 2.5 times higher than that of the composition N0_SPP_LP0.6 and 1.5 times lower than N0_CA_LP0.6. The concentration increased rapidly, reaching the same values as the concentration of Ca^{2+} ions in the composition N0_SP_CA_LP0.6 by 72 h.

In the series N0-N20-N40-N60, the concentration of Ca^{2+} ions decreased slightly for all periods of immersion of the ceramics in saline, and the concentration of Mg^{2+} increased. The concentration of Mg^{2+} in the contact solution of the composition N60_LP0.7 significantly exceeded the concentration of Mg^{2+} in the contact solutions of the compositions N20_LP0.7 and N40_LP0.7 at all incubation periods. The Mg/Ca ratio in saline solution exceeded the values calculated from the reaction, which indicates a faster dissolution of the magnesium-containing phase of newberyite and possibly other calcium magnesium phosphates, compared with calcium phosphate phases. The Mg/Ca ratio increased over time for all formulations and varied from 0.92 to 1.56 for N20_LP0.7, from 1.80 to 2.00 for N40_LP0.7, and from 4.33 to 5.13 for N60_LP0.7, and the Mg/Ca ratio for the reaction was 0.23, 0.62, and 1.36, respectively.

The microstructure of ceramics without magnesium ions almost did not change during incubation in the saline solution (Figure 8). Clusters of small crystals on the surface of large crystals of brushite and monetite formed when the solution was supersaturated inside the pores during incubation. With the introduction of the CA additive, a large number of small crystals were observed. In the compositions of N40_LP0.7 and N60_LP0.7, significant defects in prismatic crystals of newberyite (shown by arrows) are visible. This is consistent with the solubility data. Deep holes formed in newberyite crystals from the side of the smaller face, and prismatic crystals of brushite and monetite appeared in the form of parallelepiped cracks (Figure 8k,l).

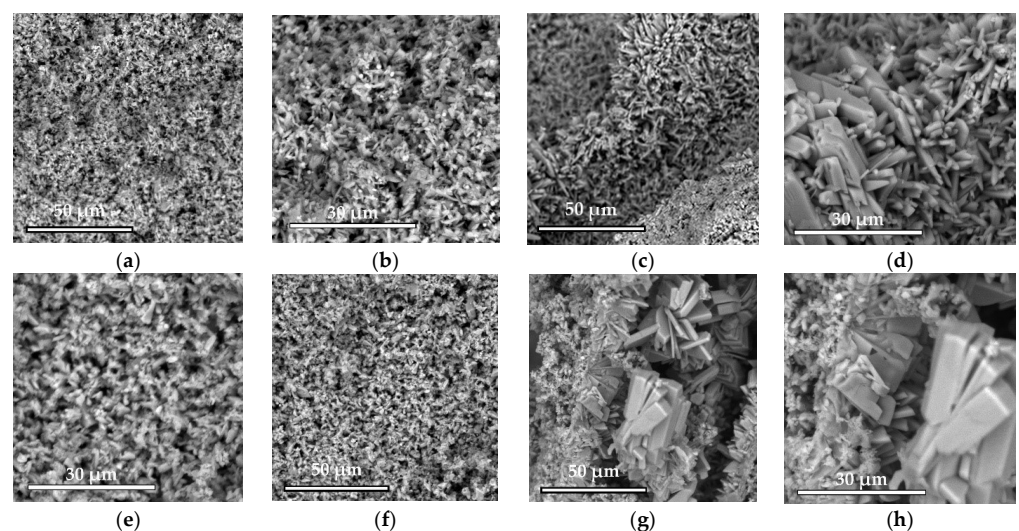


Figure 8. Cont.

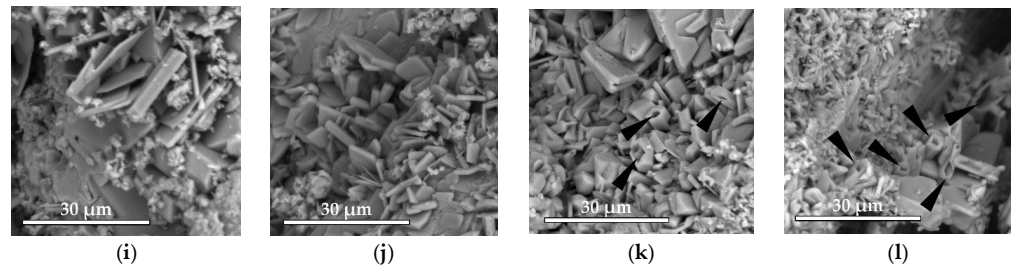
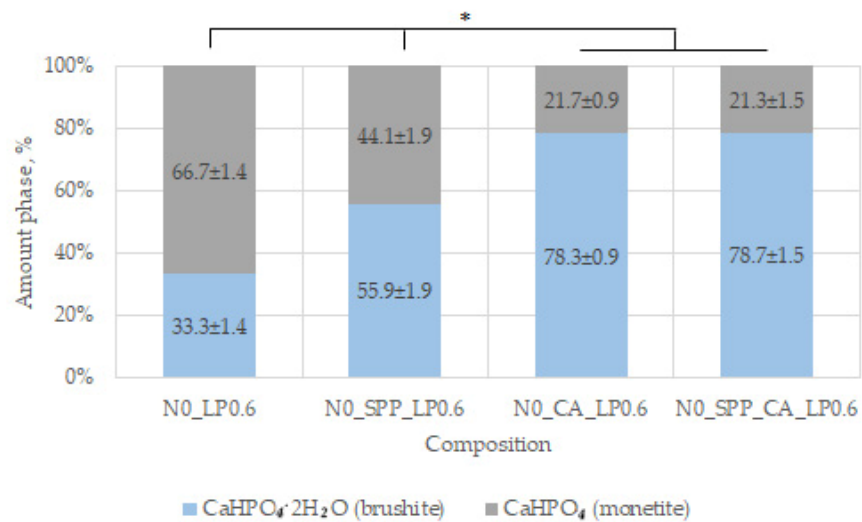
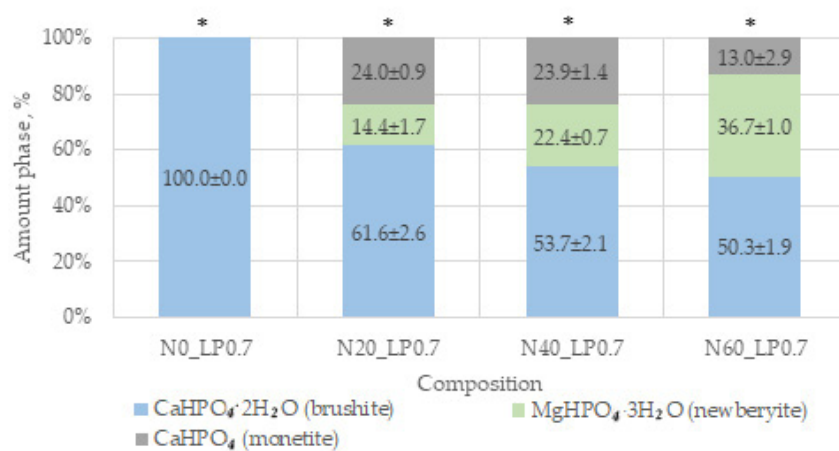


Figure 8. Micrographs of ceramics after physiological solution: N0_LP0.6 (a–d); N0_SPP_LP0.6 (e,f); N0_CA_LP0.6 (g,h); N0_LP0.7 (i); N20_LP0.7 (j); N40_LP0.7 (k); N60_LP0.7 (l). Magnification $\times 2500$ for (a,c,e,g). Magnification $\times 5000$ for (b,d,f,h–l).

A quantitative analysis of the phase composition of incubated ceramics is shown in Figure 9. The ratio of the phases of monetite and brushite after the incubation of ceramics in saline solution did not change for the composition N0_LP0.6. The amount of brushite increased slightly in incubated formulations with the introduction of SP, and it increased by about 17% with the introduction of CA or SPP_CA together.



(a)



(b)

Figure 9. Quantitative phase composition of ceramics: (a) N0 when setting retarders are introduced, (b) magnesium containing SPP and CA after incubation of physiological solution. Significant differences are labeled with * ($p < 0.05$).

It can be assumed that recrystallization occurred when the ceramics were immersed in saline, since the solubility of magnetite is less than brushite. During incubation for 7 days, the amount of the newberyite phase in the ceramics decreased, and the difference in the amount of phase in the N20-N40-N60 series increased. This fact once again confirms the unequal dissolution of phases in an aqueous medium.

3.2.5. Cell Viability Test

Figure 10 shows the results of a cell viability test in direct contact.

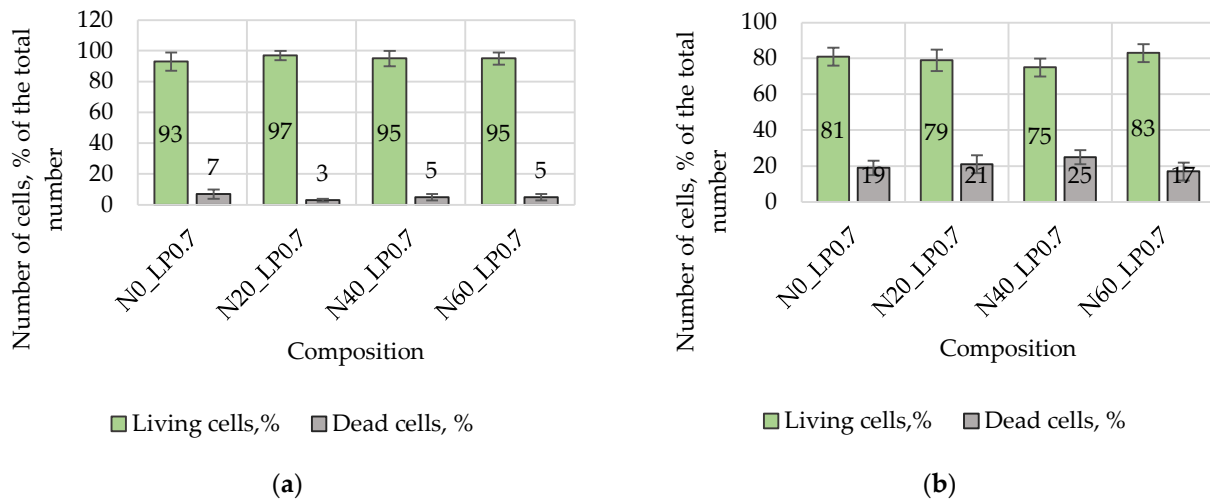


Figure 10. Cytotoxic effect of ceramics after 24 (a) and 96 h (b) of cultivating mesenchymal stromal cells of human bone marrow on them.

All samples of magnesium calcium phosphate materials had no cytotoxicity after 24 h of cultivating human bone marrow mesenchymal stromal cells on them. After 96 h of cultivation, all materials had no pronounced cytotoxic effect. The maximum number of dead cells when cultured with the study samples did not exceed $25 \pm 4\%$ of the total number of cells.

3.3. In Vivo Experiments

The biocompatibility and resorption rate of the magnesium calcium phosphate ceramics N0, N20, N40, N60 were studied in in vivo experiments on Wistar rats in a subcutaneous implantation model. In order to study the effect of setting inhibitor additives on the rate of resorption, the test animals were divided into three groups, differing in the additive that was introduced into all cement compositions: (1) SPP, (2) CA, or (3) SPP_CA.

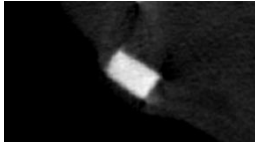
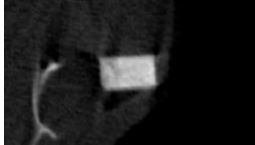
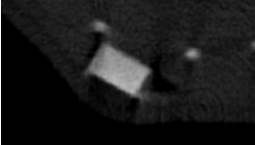
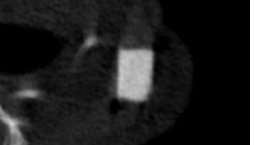
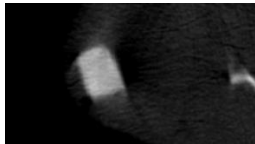
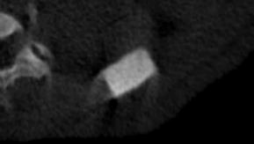
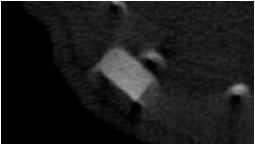
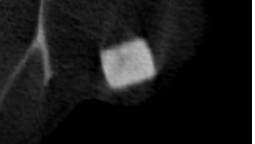
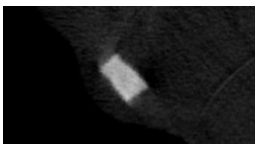
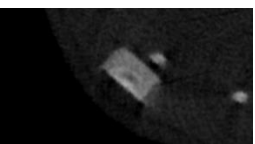
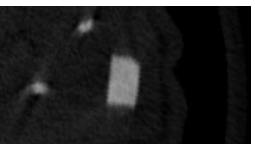
3.3.1. X-ray Density of Ceramics

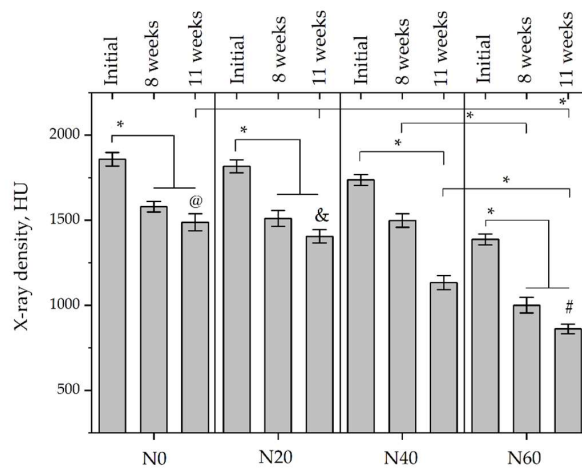
To determine the rate of resorption of materials, the values of X-ray density on the Hounsfield scale (HU) were used.

The results of the study are presented in Tables 5–7 and Figure 11.

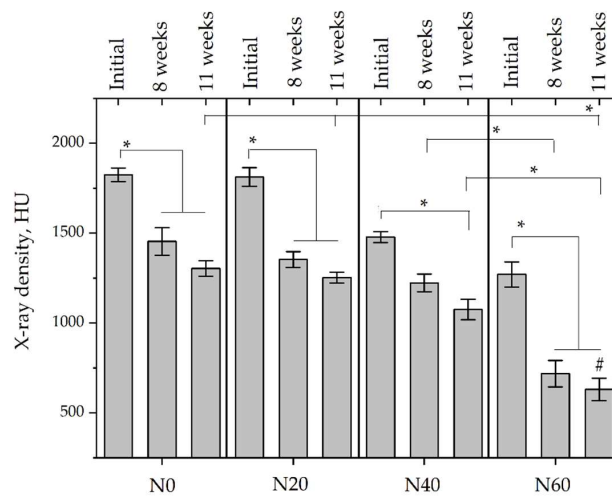
The initial radiological density decreased in the range of N0-N20-N40-N60, which indicates a lower radiological density of newberyite compared to calcium phosphates. A decrease in the X-ray density from time to time is a characteristic of all samples of magnesium calcium phosphate materials. An increase in the amount of magnesium in the composition of ceramics led to a greater decrease in X-ray density: 20–30% for N0, 23–35% for N20, 27–37% for N40, and 38–51% for N60. The highest percentage of resorption was generally characteristic of compositions with CA as the setting inhibitor and the lowest for compositions with SPP. At weeks 8 and 11, there was some compaction inside the samples N60_CA_LP0.7 and N60_SPP_CA_LP0.7, respectively.

Table 5. Examples of X-ray micrographs for ceramics with SPP and X-ray density (HU) of the implants immediately after implantation (initial), after 8 weeks, and after 11 weeks in situ.

| | N0_SPP_LP0.7 | N20_SPP_LP0.7 | N40_SPP_LP0.7 | N60_SPP_LP0.7 |
|----------|---|---|--|---|
| Initial |  |  |  |  |
| 8 weeks |  |  |  |  |
| 11 weeks |  |  |  |  |



(a)



(b)

Figure 11. Cont.

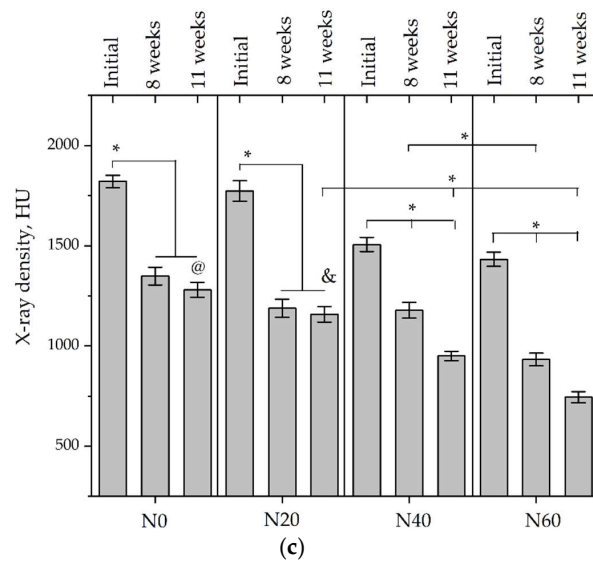
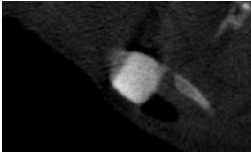
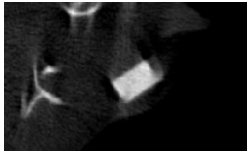
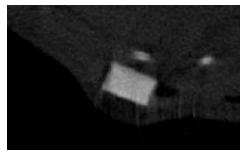
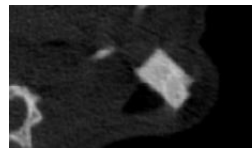
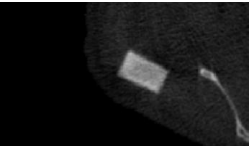
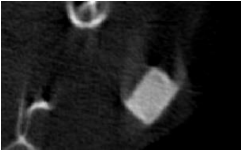
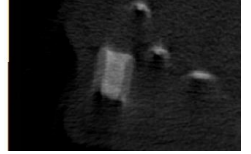
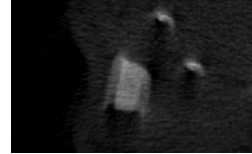
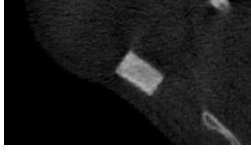
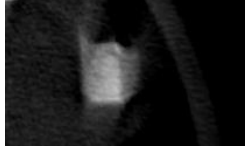
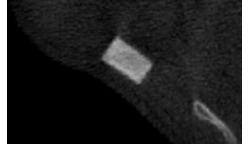
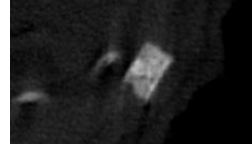


Figure 11. X-ray density (HU) for ceramic implants with set-retarding additives immediately after implantation (initial), after 8 weeks, and after 11 weeks in situ: (a) with PPS; (b) with CA; (c) with CA_PPS. Significant differences ($p < 0.05$) between different materials at one time point are labeled with *, and significant differences at a specific time point between different groups are labeled with #, @, and &.

Table 6. Examples of X-ray micrographs for ceramics with CA and X-ray density (HU) of the implants immediately after implantation (initial), after 8 weeks, and after 11 weeks in situ.

| | N0_CA_LP0.7 | N20_CA_LP0.7 | N40_CA_LP0.7 | N60_CA_LP0.7 |
|----------|-------------|--------------|--------------|--------------|
| Initial | | | | |
| 8 weeks | | | | |
| 11 weeks | | | | |

Table 7. Examples of X-ray micrographs for ceramics with SPP_CA and X-ray density (HU) of the implants immediately after implantation (initial), after 8 weeks, and after 11 weeks in situ.

| | N0_SPP_CA_LP0.7 | N20_SPP_CA_LP0.7 | N40_SPP_CA_LP0.7 | N60_SPP_CA_LP0.7 |
|----------|---|---|--|---|
| Initial |  |  |  |  |
| 8 weeks |  |  |  |  |
| 11 weeks |  |  |  |  |

3.3.2. Phase Compositions and Microstructures of Ceramics after Implantation

Most of the X-ray density was lost during the resorption of the newberyite phase from the ceramic’s composition, the absence of which at week 11 was confirmed by X-ray phase analysis data (Figure 12).

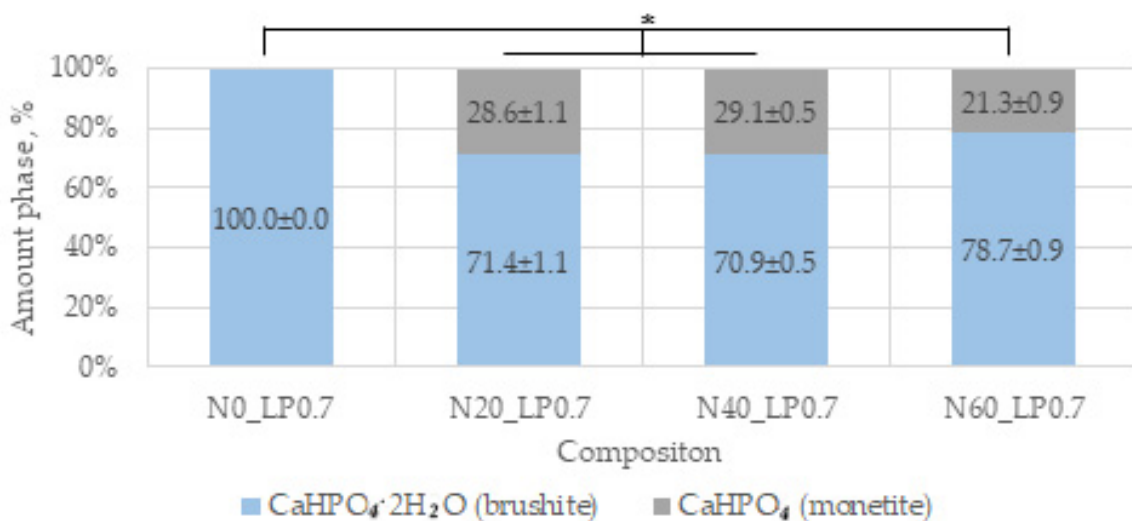


Figure 12. Quantitative phase composition of ceramics after implantation. Significant differences are labeled with * ($p < 0.05$).

The microstructure of ceramics after implantation was looser, represented by small crystals (Figure 13). There were no large crystals present in the structure of ceramics before implantation. It is rare to find crystals of brushite with a size of 10–15 microns, which in most cases are defective. A single cluster of crystals similar to newberyite crystals, almost completely dissolved, was found in a sample of the composition N60_SP_CA_LP0.7.

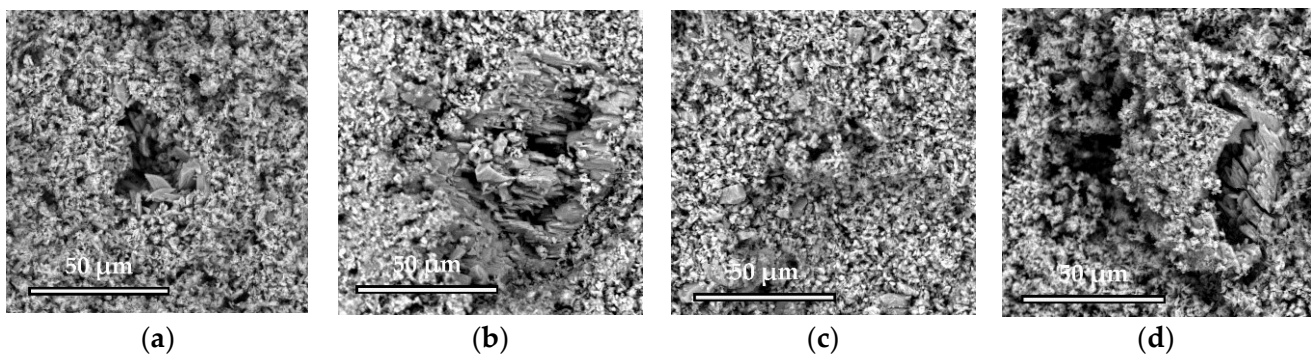


Figure 13. Micrographs of ceramics: N0_SPP_CA_LP0.7 (a), N20_SPP_CA_LP0.7 (b), N40_SPP_CA_LP0.7 (c), N60_SPP_CA_LP0.7 (d). Magnification $\times 2500$.

3.3.3. Morphological Study of Connective Tissue Capsules

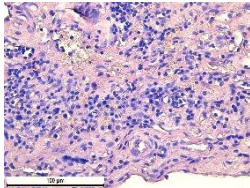
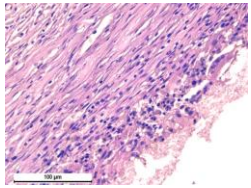
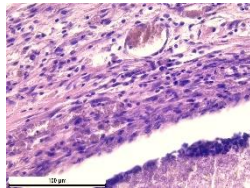
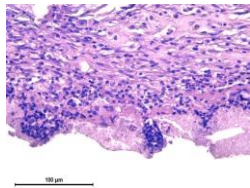
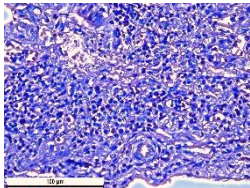
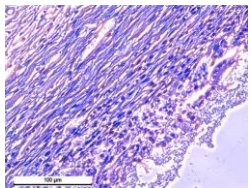
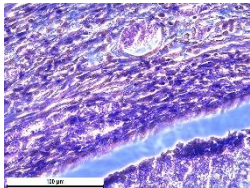
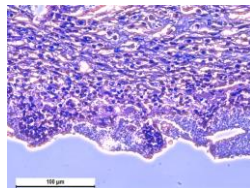
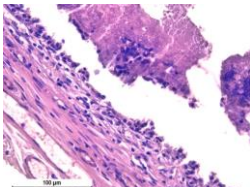
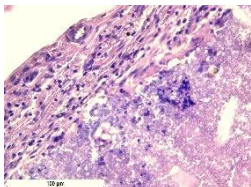
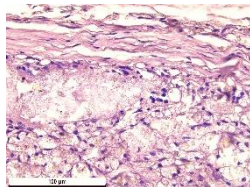
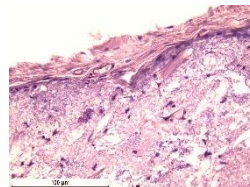
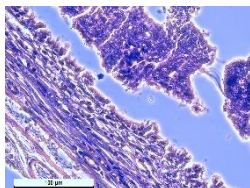
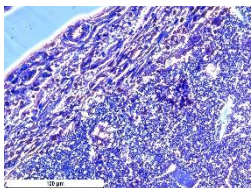
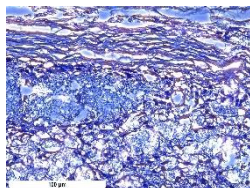
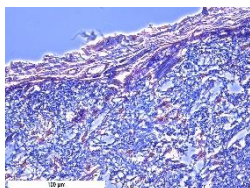
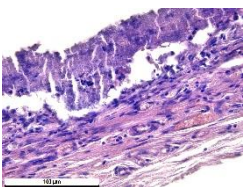
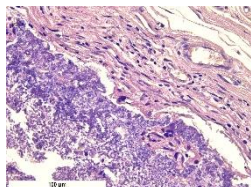
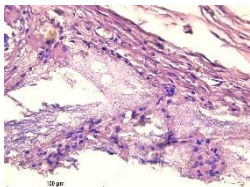
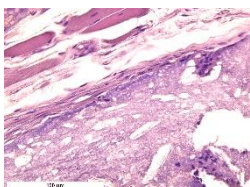
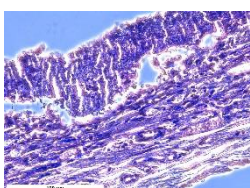
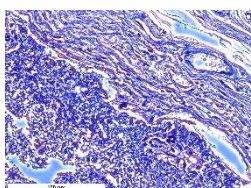
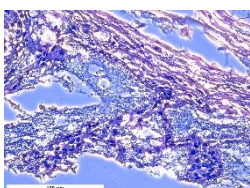
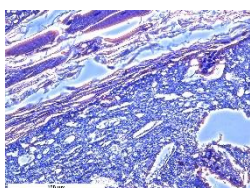
Photographs of sections of the samples under study under various microscopy modes are shown in Table 8. Table 9 shows the distribution of the relative area of vessels (per 100 thousand μm^2 of capsule area) for samples of magnesium calcium phosphate ceramics containing SPP, CA, and SPP_CA.

Sufficiently thick mature fibrous capsules with an increased content of vessels and pronounced inflammatory infiltration with a predominance of lymphocytes and neutrophils were mainly formed during implantation of samples of magnesium calcium phosphate ceramics of different compositions containing SPP. At the same time, the implant resorption was marginal with the penetration of single macrophages deep into the implant.

Only marginal resorption without penetration of macrophages deep into the implant was observed in the ceramic samples N0_CA and N0_SPP_CA. The introduction of single macrophages into the implant for composition N20, with a gradual increase for samples N40 and N60, was observed when newberyite appeared in the composition of the ceramics. Thinner capsules with less pronounced vascularization and inflammatory infiltration were formed during implantation of the magnesium calcium phosphate ceramic samples of different compositions with CA and SPP_CA. Compounds N40 and N60 actively germinated with fibroblasts.

The minimum relative area of vessels and capsule thickness is a characteristic of samples with CA, which confirms their biocompatibility. Biocompatibility increases in the range N0-N20-N40-N60 with all variants of setting inhibitors. Ceramics of the compositions N40_CA, N60_CA, N40_SPP_CA, and N60_SPP_CA have higher biocompatibility and resorption. The most mature thin fibrous capsule with moderate vascular content and weak inflammatory infiltration was observed. At the same time, intensive resorption of the implant by macrophages, giant multinucleated cells, and germination of ceramics by fibroblasts were observed.

Table 8. Section photos for the studied samples at different microscopy modes.

| | | N0_LP0.7 | N20_LP0.7 | N40_LP0.7 | N60_LP0.7 |
|--------|-----|---|---|--|---|
| SPP | SLM |  |  |  |  |
| | PCM |  |  |  |  |
| CA | SLM |  |  |  |  |
| | PCM |  |  |  |  |
| CA_SPP | SLM |  |  |  |  |
| | PCM |  |  |  |  |

SLM—standard light microscopy. PCM—phase-contrast microscopy. Hematoxylin-eosin, magnification 400×.

Table 9. The average thickness of fibrous capsules (μm) and the relative area of vessels per 100 thousand μm^2 of capsule area. *—significant differences.

| Composition | N0_LP0.7 | | | N20_LP0.7 | | | N40_LP0.7 | | | N60_LP0.7 | | |
|--|-------------------|----------------------|--------------------|--------------------|-------------------|------------------|--------------------|----------------------|--------------------|-------------------|-------------------|--------------------|
| | SPP | CA | SPP_CA | SPP | CA | SPP_CA | SPP | CA | SPP_CA | SPP | CA | SPP_CA |
| Capsule thickness, μm | 602.6 \pm 88.2 | 108.0 * \pm 6.9 | 123 \pm 15.9 | 299.9 \pm 15.1 | 104.4 * \pm 7.1 | 116.7 \pm 8.4 | 531.1 \pm 35.1 | 90.3 * \pm 3.6 | 104.7 \pm 5.9 | 213.9 \pm 30.7 | 66.5 * \pm 4.4 | 78.6 \pm 2.9 |
| <i>p</i> -level | <0.0001 | | | <0.0001 | | | <0.0001 | | | 0.0002 | | |
| Vessel area, $\mu\text{m}^2/100,000 \mu\text{m}^2$ | 857.4 \pm 303.5 | 4547.0 * \pm 529.7 | 3973.2 \pm 418.6 | 4130.0 \pm 646.1 | 3525 \pm 309.2 | 3821 \pm 291.1 | 4394.0 \pm 304.6 | 2825.0 * \pm 445.9 | 3282.1 \pm 234.8 | 5720.0 \pm 1959 | 3259.0 \pm 1345 | 2978.5 \pm 245.3 |
| <i>p</i> -level | 0.004 | | | 0.408 | | | 0.008 | | | 0.306 | | |

4. Discussion

Magnesium was introduced into the initial component of TCP brushite cement until $\text{Mg}_x\text{Ca}_{(3-x)}(\text{PO}_4)_2$ was obtained at $x = 0, 0.75, 1.5, 2.25$ in order to obtain uniformly magnesium-doped brushite and newberyite.

The diffraction peaks of the Mg0.75 composition shift towards larger values of the angle 2Θ compared to Mg0, and new peaks of low intensity appear, related to $\text{Mg}_3\text{Ca}_3(\text{PO}_4)_4$.

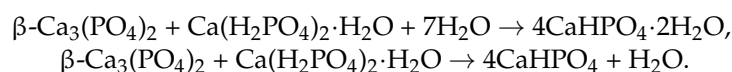
Saleh et al. did not find phases other than β -TCP in the composition of $\text{Ca}_{(8.88-x)}\text{Mg}_x(\text{PO}_4)_6$ when x was less than 1 [33]. However, the incorporation of Mg^{2+} into the β -TCP lattice led to a shift in the diffraction peaks $d = 2.61, 2.88, 3.21 \text{ \AA}$ to higher values of 2Θ [41], as well as a decrease in the intensity of X-ray peaks, which was attributed to the substitution of Ca^{2+} ions of larger size (1.00 \AA) for Mg^{2+} ions of smaller size (0.72 \AA) [42].

According to the literature data, the maximum amount of magnesium capable of replacing calcium in the positions of Ca(4) and Ca(5) in the TCP structure is 14–15 mol.% [42,43]. Exceeding 15.00 mol.% Mg^{2+} leads to the formation of a magnesium-rich phase, such as stanfieldite [42].

In our case, the concentration of doped magnesium was higher than 25 mol.% (Mg0.75). In this regard, magnesium ions were embedded in the TCP structure, and an additional phase of magnesium calcium phosphate $\text{Mg}_3\text{Ca}_3(\text{PO}_4)_4$ was formed, which became the only phase when the magnesium increased to 1.5. A further increase in magnesium leads to the formation of $\text{Mg}_3(\text{PO}_4)_2$ trimagnesium phosphate.

Low-temperature magnesium calcium phosphate ceramics were obtained by cement technology through the acid–base interaction of $\text{Mg}_x\text{Ca}_{(3-x)}(\text{PO}_4)_2$ and monocalcium phosphate monohydrate $\text{Ca}(\text{H}_2\text{PO}_4)_2 \cdot \text{H}_2\text{O}$ (MCPM).

The main phases of the magnesium-free ceramics are brushite $\text{CaHPO}_4 \cdot 2\text{H}_2\text{O}$ and monetite CaHPO_4 , in accordance with the equations:



Brushite is more soluble ($-\log(K_{\text{sp}}) = 6.59$) than monetite ($-\log(K_{\text{sp}}) = 6.90$), and it formed faster as a result of the reaction [44]. In our work, additive-free ceramics contain about 30% brushite, which we attribute to a lack of cement-mixing fluid due to the small particle size of the initial component, which increases the water requirement.

With the introduction of set-retarding additives and increasing the water/solid ratio, the amount of the brushite phase increases.

Monetite, on the one hand, is an undesirable phase of ceramics due to a decrease in strength in its presence and a lower dissolution rate [45]. On the other hand, when aging in an aqueous medium or subcutaneously, monetite, unlike brushite, does not transform into other poorly soluble phases [27,46], and therefore, it was characterized by a higher rate of resorption [31,44].

A slight difference in the amount of newberyite formed in the compositions of N20, N40, and N60 from the target values was associated, in our opinion, with the expenditure of magnesium on the doping of the brushite phase.

An increase in setting time and compressive strength was observed by Saleh et al. with an increase in the magnesium content in brushite cement. The initial setting time increased to 33 min with a magnesium content of up to 10% in the composition of TCP [33]. In our work, the beginning of setting of the additive-free cement was less than 30 s for all Mg-substituted compounds. However, we found that the number of setting inhibitors was required less with an increase in the amount of magnesium in the cement composition. This may be due to the faster formation of poorly soluble $Mg_2P_2O_7$ on the surface of the new phases. An increase in the amount of magnesium in the composition of ceramics leads to a slight increase in strength and a decrease in porosity. This is consistent with the results of Alkhraisat et al., and it is connected with the formation of newberyite in the composition of ceramics, which compacts the matrix [23].

In general, SPP has a negative effect on mechanical strength, although porosity was slightly reduced. SPP probably leads to the formation of calcium and magnesium pyrophosphates on the surface of the particles, partially preventing the formation of contacts of the mineral component of the consolidated matrix, which leads to a decrease in mechanical strength. CA seals the ceramic structure, reduces porosity, and significantly reduces pH. The combined use of additives reduces the negative effect when used separately and is preferable.

An increase in the liquid/solid ratio leads to an increase in porosity to values without additional ceramics. The phase composition of ceramics containing newberyite was not affected by an increase in L/P.

Set-retarding additives and magnesium doping have an effect on the solubility of ceramics. The amount of calcium ions in the contact medium was less than the amount of magnesium ions and almost did not differ for all compositions. CA increases the solubility of ceramics by six times in the initial period and by one and a half times by 5 days. Perhaps this is due to the formation of calcium citrate and a decrease in the size of ceramic particles. SPP reduces the level of calcium released into the solution in the first 24 h, after which the amount of calcium ions increases and reaches values greater than those for non-additive ceramics.

The release of Mg^{2+} ions from ceramic samples N20, N40, and N60 for 5 days increased with an increase in the amount of magnesium in the precursor due to a lower degree of crystallinity of alloyed ceramic samples and the content of newberite, which has a greater chemical solubility ($-\log(K_{sp}) = 5.51-5.82$) than brushite and monetite. After 7 days, the amount of newberite in the ceramic composition decreased significantly. The higher dissolution rate of magnesium-substituted brushite is consistent with the data of Alkhraisat et al. They observed an excess of Mg^{2+} magnesium ions in SBF solution over Ca^{2+} calcium ions and an increase in solubility in general with an increase in the magnesium content in the cement composition [23]. A more intense dissolution of newberyite compared to brushite was observed by Klammert et al. during subcutaneous implantation in rats in *in vivo* experiments [17].

In our study, a model of subcutaneous implantation in rats was also chosen. Since the implants were surrounded only by soft tissues, it was easy to carry out X-ray monitoring of the solubility of the implant without harming animals in long-term experiments. Changes in the phase composition can be investigated due to the absence of ingrown (and mineral-containing) hard tissues [17].

According to micro-CT, the surface resorption of ceramic granules was very insignificant, whereas dissolution was observed throughout the entire volume of ceramics, as can be judged by the X-ray density data. In our studies, the X-ray density of ceramics by the 8th and 11th days of implantation was less than the initial density. The mechanism of reducing the X-ray density of ceramics based on brushite and newberyite is associated with more intensive dissolution of the newberyite phase (Mg^{2+} and HPO_4^{2-}) and less intensive dissolution of the brushite/monetite phase (Ca^{2+} and HPO_4^{2-}) throughout the volume and leaching from the implant.

At week 8 and 11, there is some compaction inside the samples N60_CA and N60_SPP_CA. The formation of radiologically denser regions is probably associated with the re-deposition of brushite during ionic supersaturation into less soluble phases of calcium phosphate [47]. However, no such compounds were found on radiographs. X-ray phase analysis of ceramic samples showed strong differences in the phase composition before and after implantation of ceramic granules. The absence of the newberyite phase in all modifications of ceramics confirms its higher dissolution rate.

Recrystallization in the center of the sample is most likely due to the highest saturation with Ca^{2+} and HPO_4^{2-} ions due to the smallest boundary with the environment [47]. Bonner et al. observed the formation of apatite at 6–8 weeks. The absence of magnesium in the composition of ceramics can contribute to recrystallization. It should be noted that the X-ray density of samples N60_CA and N60_SPP_CA was lower than N60_SPP. Ceramics containing SPP did not show areas with a higher X-ray density in the center of the ceramics. SPP forms magnesium and calcium pyrophosphate, which are less soluble than brushite, monetite, and newberyite [47]. The literature data on the prevention of brushite recrystallization with the introduction of pyrophosphate are in contradiction to each other [48,49].

In addition to passive resorption due to chemical dissolution, active (cell-mediated) resorption due to the presence of macrophages was also observed in in vivo experiments [45,50,51]. Further, the presence of macrophages indirectly confirms the absence of brushite recrystallization, in which active resorption occurs exclusively by osteoclasts [31].

Animal studies using a subcutaneous implantation model have confirmed the assumption of volumetric dissolution of magnesium calcium phosphate ceramics and their biocompatibility. The rate of dissolution directly depends on the amount of magnesium in the composition and on the setting-inhibitor additive used. It was found that SPP reduces the rate of dissolution and biocompatibility, but not critically. The joint use of SPP and CA is optimal in terms of the physical and chemical properties of ceramics and biocompatibility. Optimal concentrations of SSP and CA additives when used together for compositions with different Mg^{2+} magnesium ion content in ceramics were found in our work. The resorption rate of ceramics based on brushite-newberyite cement can be controlled by the amount of Mg^{2+} ions. The main advantage of the resulting multiphase ceramics is volumetric resorption due to the different dissolution rates of the phases and the possibility of germination of the surrounding tissue into the internal space formed by dissolution. This was confirmed by the germination of fibroblasts during subcutaneous implantation.

An in vivo study of subcutaneous implantation confirms the biocompatibility and different rates of resorption of magnesium-calcium phosphate ceramics containing various setting inhibitors and determines the vector of further studies of magnesium-calcium phosphate ceramics, including in orthotopic implantation models.

5. Conclusions

An increase in the amount of the magnesium ion Mg^{2+} in the composition of TCP leads to a slight increase in the strength and a decrease in the porosity of ceramics based on brushite-newberyite cement, as well as a significant increase in volume solubility due to the primary dissolution of the newberyite phase. SPP negatively affects the solubility, mechanical strength, and biocompatibility of ceramics. CA seals the ceramic structure, reduces porosity, increases strength, and significantly reduces pH. The combined use of additives is preferable for achieving optimal properties of ceramics.

We have demonstrated the possibility of regulating the rate of volumetric resorption of low-temperature ceramics based on brushite-newberyite cement containing setting inhibitors by changing the amount of magnesium in the initial TCP.

Author Contributions: Conceptualization, Y.L.; methodology, Y.L., N.G. and S.S.; investigation, Y.L., S.K., L.B.-A., N.S., R.C., R.F., O.T., A.T., M.R. and D.S.; writing—original draft preparation, Y.L.; writing—review and editing, Y.L.; visualization, Y.L., L.B.-A., N.S., R.F., A.T. and M.R.; supervision,

Y.L.; project administration, Y.L. All authors have read and agreed to the published version of the manuscript.

Funding: This research was carried out within the framework of the state task “Development of technology for obtaining osteoplastic polymer and calcium phosphate materials with a controlled rate of release of antibiotics and targeted pharmaceutical substances for the surgical treatment of purulent processes of bone tissue and prevention of the formation of bacterial biofilms on implantable metal structures” and was funded by the Ministry of Health of the Russian Federation.

Institutional Review Board Statement: The protocol of the animal study was approved by the Local Ethical Committee for Medical and Biological Ethics of the N.N. Priorov National Medical Research Center for Traumatology and Orthopedics of the Ministry of Health of the Russian Federation (protocol code 002, approval date 2 February 2022).

Informed Consent Statement: Not applicable.

Data Availability Statement: Not applicable.

Acknowledgments: The authors wish to give thanks for the use of the equipment of the Shared Research Center “Analytical center of deep oil processing and petrochemistry of TIPS RAS”.

Conflicts of Interest: The authors declare no conflict of interest. The funders had no role in the design of the study; in the collection, analyses, or interpretation of data; in the writing of the manuscript; or in the decision to publish the results.

References

1. Padalhin, A.R.; Kim, B.; Ventura, R.D.; Lee, H.J.; Lee, S.J.; Lee, B.-T. Development of fibrous balloon for facilitating the use of calcium phosphate cement in vertebral augmentation procedures. *Mater. Des.* **2018**, *158*, 172–183. [[CrossRef](#)]
2. Thein-Han, W.; Liu, J.; Xu, H.H. Calcium phosphate cement with biofunctional agents and stem cell seeding for dental and craniofacial bone repair. *Dent. Mater.* **2012**, *28*, 1059–1070. [[CrossRef](#)] [[PubMed](#)]
3. Mestres, G.; Kugiejko, K.; Pastorino, D.; Unosson, J.; Öhman, C.; Ott, M.K.; Ginebra, M.-P.; Persson, C. Changes in the drug release pattern of fresh and set simvastatin-loaded brushite cement. *Mater. Sci. Eng. C* **2016**, *58*, 88–96. [[CrossRef](#)] [[PubMed](#)]
4. Sun, R.; Åhlén, M.; Tai, C.-W.; Bajnóczi, G.; de Kleijne, F.; Ferraz, N.; Persson, I.; Strømme, M.; Cheung, O. Highly porous amorphous calcium phosphate for drug delivery and bio-medical applications. *Nanomaterials* **2019**, *10*, 20. [[CrossRef](#)] [[PubMed](#)]
5. Xia, W.; Mohd Razi, M.R.; Ashley, P.; Abou Neel, E.A.; Hofmann, M.P.; Young, A.M. Quantifying effects of interactions between polyacrylic acid and chlorhexidine in dicalcium phosphate-forming cements. *J. Mater. Chem. B* **2014**, *2*, 1673–1680. [[CrossRef](#)] [[PubMed](#)]
6. Pujari-Palmer, M.; Pujari-Palmer, S.; Engqvist, H.; Karlsson Ott, M. Rebamipide delivered by brushite cement enhances osteoblast and macrophage proliferation. *PLoS ONE* **2015**, *10*, e0128324. [[CrossRef](#)] [[PubMed](#)]
7. Hurle, K.; Oliveira, J.M.; Reis, R.L.; Pina, S.; Goetz-Neunhoffer, F. Ion-doped brushite cements for bone regeneration. *Acta Biomater.* **2021**, *123*, 51–71. [[CrossRef](#)]
8. Nasrollahi, N.; Dehkordi, A.N.; Jamshidizad, A.; Chehelgerdi, M. Preparation of brushite cements with improved properties by adding graphene oxide. *Int. J. Nanomed.* **2019**, *14*, 3785–3797. [[CrossRef](#)]
9. Roy, M.; DeVoe, K.; Bandyopadhyay, A.; Bose, S. Mechanical property and in vitro biocompatibility of brushite cement modified by polyethylene glycol. *Mater. Sci. Eng. C* **2012**, *32*, 2145–2152. [[CrossRef](#)]
10. Hofmann, M.P.; Mohammed, A.R.; Perrie, Y.; Gbureck, U.; Barralet, J.E. High-strength resorbable brushite bone cement with controlled drug-releasing capabilities. *Acta Biomater.* **2009**, *5*, 43–49. [[CrossRef](#)]
11. Tamimi, F.; Torres, J.; Bettini, R.; Ruggera, F.; Rueda, C.; López-Ponce, M.; Lopez-Cabarcos, E. Doxycycline sustained release from brushite cements for the treatment of periodontal diseases. *J. Biomed. Mater. Res. Part A* **2007**, *85*, 707–714. [[CrossRef](#)]
12. Young, A.M.; Ng, P.Y.J.; Gbureck, U.; Nazhat, S.N.; Barralet, J.E.; Hofmann, M.P. Characterization of chlorhexidine-releasing, fast-setting, brushite bone cements. *Acta Biomater.* **2008**, *4*, 1081–1088. [[CrossRef](#)] [[PubMed](#)]
13. Tamimi, F.; Sheikh, Z.; Barralet, J. Dicalcium phosphate cements: Brushite and monetite. *Acta Biomater.* **2012**, *8*, 474–487. [[CrossRef](#)]
14. Kim, J.-A.; Lim, J.; Naren, R.; Yun, H.-S.; Park, E.K. Effect of the biodegradation rate controlled by pore structures in magnesium phosphate ceramic scaffolds on bone tissue regeneration in vivo. *Acta Biomater.* **2016**, *44*, 155–167. [[CrossRef](#)] [[PubMed](#)]
15. Kanter, B.; Vikman, A.; Brückner, T.; Schamel, M.; Gbureck, U.; Ignatius, A. Bone regeneration capacity of magnesium phosphate cements in a large animal model. *Acta Biomater.* **2018**, *69*, 352–361. [[CrossRef](#)] [[PubMed](#)]
16. Sayahi, M.; Santos, J.; El-Feki, H.; Charvillat, C.; Bosc, F.; Karacan, I.; Milthorpe, B.; Drouet, C. Brushite (Ca,M)HPO₄·2H₂O doping with bioactive ions (M = Mg²⁺, Sr²⁺, Zn²⁺, Cu²⁺, and Ag⁺): A new path to functional biomaterials? *Mater. Today Chem.* **2020**, *16*, 100230. [[CrossRef](#)]
17. Klammert, U.; Ignatius, A.; Wolfram, U.; Reuther, T.; Gbureck, U. In vivo degradation of low temperature calcium and magnesium phosphate ceramics in a heterotopic model. *Acta Biomater.* **2011**, *7*, 3469–3475. [[CrossRef](#)]

18. Lee, D.; Kumta, P.N. Chemical synthesis and stabilization of magnesium substituted brushite. *Mater. Sci. Eng. C* **2010**, *30*, 934–943. [[CrossRef](#)]
19. Cacciotti, I.; Bianco, A. High thermally stable Mg-substituted tricalcium phosphate via precipitation. *Ceram. Int.* **2011**, *37*, 127–137. [[CrossRef](#)]
20. Cabrejos-Azama, J.; Alkhraisat, M.H.; Rueda, C.; Torres, J.; Blanco, L.; López-Cabarcos, E. Magnesium substitution in brushite cements for enhanced bone tissue regeneration. *Mater. Sci. Eng. C* **2014**, *43*, 403–410. [[CrossRef](#)]
21. Klammert, U.; Reuther, T.; Blank, M.; Reske, I.; Barralet, J.E.; Grover, L.M.; Kübler, A.C.; Gbureck, U. Phase composition, mechanical performance and in vitro biocompatibility of hydraulic setting calcium magnesium phosphate cement. *Acta Biomater.* **2010**, *6*, 1529–1535. [[CrossRef](#)]
22. Pina, S.; Torres, P.M.C.; Ferreira, J.M.F. Injectability of brushite-forming Mg-substituted and Sr-substituted α -TCP bone cements. *J. Mater. Sci. Mater. Electron.* **2009**, *21*, 431–438. [[CrossRef](#)] [[PubMed](#)]
23. Alkhraisat, M.H.; Cabrejos-Azama, J.; Rodríguez, C.R.; Jerez, L.B.; Cabarcos, E.L. Magnesium substitution in brushite cements. *Mater. Sci. Eng. C* **2013**, *33*, 475–481. [[CrossRef](#)] [[PubMed](#)]
24. TenHuisen, K.S.; Brown, P.W. Effects of magnesium on the formation of calcium-deficient hydroxyapatite from $\text{CaHPO}_4 \cdot 2\text{H}_2\text{O}$ and $\text{Ca}_4(\text{PO}_4)_2\text{O}$. *J. Biomed. Mater. Res.* **1997**, *36*, 306–314. [[CrossRef](#)]
25. Kanzaki, N.; Onuma, K.; Treboux, G.; Ito, A. Dissolution kinetics of dicalcium phosphate dihydrate under pseudophysiological conditions. *J. Cryst. Growth* **2002**, *235*, 465–470. [[CrossRef](#)]
26. Sheikh, Z.; Najeeb, S.; Khurshid, Z.; Verma, V.; Rashid, H.; Glogauer, M. Biodegradable materials for bone repair and tissue engineering applications. *Materials* **2015**, *8*, 5744–5794. [[CrossRef](#)] [[PubMed](#)]
27. Sheikh, Z.; Zhang, Y.L.; Grover, L.; Merle, G.E.; Tamimi, F.; Barralet, J. In vitro degradation and in vivo resorption of dicalcium phosphate cement based grafts. *Acta Biomater.* **2015**, *26*, 338–346. [[CrossRef](#)] [[PubMed](#)]
28. Sheikh, Z.; Geffers, M.; Christel, T.; Barralet, J.E.; Gbureck, U. Chelate setting of alkali ion substituted calcium phosphates. *Ceram. Int.* **2015**, *41*, 10010–10017. [[CrossRef](#)]
29. Gallo, M.; Tadier, S.; Meille, S.; Gremillard, L.; Chevalier, J. The in vitro evolution of resorbable brushite cements: A physico-chemical, micro-structural and mechanical study. *Acta Biomater.* **2017**, *53*, 515–525. [[CrossRef](#)]
30. Rousseau, S.; Lemaître, J.; Bohner, M.; Frei, C. Long-term aging of brushite cements in physiological conditions: An in vitro study. *Eur. Cells Mater.* **2002**, *5*, 2.
31. Sheikh, Z.; Abdallah, M.-N.; Hanafi, A.A.; Misbahuddin, S.; Rashid, H.; Glogauer, M. Mechanisms of in vivo degradation and resorption of calcium phosphate based biomaterials. *Materials* **2015**, *8*, 7913–7925. [[CrossRef](#)] [[PubMed](#)]
32. Sikder, P.; Ren, Y.; Bhaduri, S.B. Microwave processing of calcium phosphate and magnesium phosphate based orthopedic bioceramics: A state-of-the-art review. *Acta Biomater.* **2020**, *111*, 29–53. [[CrossRef](#)] [[PubMed](#)]
33. Saleh, A.T.; Ling, L.S.; Hussain, R. Injectable magnesium-doped brushite cement for controlled drug release application. *J. Mater. Sci.* **2016**, *51*, 7427–7439. [[CrossRef](#)]
34. Bohner, M.; Merkle, H.P.; Van Landuyt, P.; Trophard, G.; Lemaître, J. Effect of several additives and their admixtures on the physico-chemical properties of a calcium phosphate cement. *J. Mater. Sci. Mater. Med.* **2000**, *11*, 111–116. [[CrossRef](#)] [[PubMed](#)]
35. Mirtchi, A.A.; Lemaître, J.; Hunting, E. Calcium phosphate cements: Action of setting regulators on the properties of the β -tricalcium phosphate-monocalcium phosphate cements. *Biomaterials* **1989**, *10*, 634–638. [[CrossRef](#)] [[PubMed](#)]
36. Penel, G.; Leroy, N.; Van Landuyt, P.; Flautre, B.; Hardouin, P.; Lemaître, J.; Leroy, G. Raman microspectrometry studies of brushite cement: In vivo evolution in a sheep model. *Bone* **1999**, *25* (Suppl. S1), 81S–84S. [[CrossRef](#)]
37. Luo, J.; Ajaxon, I.; Ginebra, M.P.; Engqvist, H.; Persson, C. Compressive, diametral tensile and biaxial flexural strength of cutting-edge calcium phosphate cements. *J. Mech. Behav. Biomed. Mater.* **2016**, *60*, 617–627. [[CrossRef](#)]
38. Hubbard, C.R.; Evans, E.H.; Smith, D.K. The reference intensity ratio, I/I_c , for computer simulated powder patterns. *J. Appl. Cryst.* **1976**, *9*, 169–174. [[CrossRef](#)]
39. Goldberg, M.A.; Krohicheva, P.A.; Fomin, A.S.; Khairutdinova, D.R.; Antonova, O.S.; Baikin, A.S.; Smirnov, V.V.; Fomina, A.A.; Leonov, A.V.; Mikheev, I.V.; et al. In situ magnesium calcium phosphate cements formation: From one pot powders precursors synthesis to in vitro investigations. *Bioact. Mater.* **2020**, *5*, 644–658. [[CrossRef](#)]
40. Zai, W.; Zhang, X.; Su, Y.; Man, H.; Li, G.; Lian, J. Comparison of corrosion resistance and biocompatibility of magnesium phosphate (MgP), zinc phosphate (ZnP) and calcium phosphate (CaP) conversion coatings on Mg alloy. *Surf. Coat. Technol.* **2020**, *397*, 125919. [[CrossRef](#)]
41. Torres, P.M.C.; Abrantes, J.C.C.; Kaushal, A.; Pina, S.; Döbelin, N.; Bohner, M.; Ferreira, J.M.F. Influence of Mg-doping, calcium pyrophosphate impurities and cooling rate on the allotropic $\alpha \leftrightarrow \beta$ -tricalcium phosphate phase transformations. *J. Eur. Ceram. Soc.* **2016**, *36*, 817–827. [[CrossRef](#)]
42. Araújo, J.C.; Sader, M.S.; Moreira, E.L.; Moraes, V.C.A.; LeGeros, R.Z.; Soares, G.A. Maximum substitution of magnesium for calcium sites in Mg- β -TCP structure determined by X-ray powder diffraction with the Rietveld refinement. *Mater. Chem. Phys.* **2009**, *118*, 337–340. [[CrossRef](#)]
43. Enderle, R.; Götz-Neunhoffer, F.; Göbbels, M.; Müller, F.; Greil, P. Influence of magnesium doping on the phase transformation temperature of β -TCP ceramics examined by Rietveld refinement. *Biomaterials* **2005**, *26*, 3379–3384. [[CrossRef](#)] [[PubMed](#)]

44. Mocanu, A.-C.; Stan, G.E.; Maidaniuc, A.; Miculescu, M.; Antoniac, I.V.; Ciocoiu, R.-C.; Voicu, I.; Mitran, V.; Cîmpean, A.; Miculescu, F. Naturally-derived biphasic calcium phosphates through increased phosphorus-based reagent amounts for biomedical applications. *Materials* **2019**, *12*, 381. [[CrossRef](#)]
45. Großardt, C.; Ewald, A.; Grover, L.M.; Barralet, J.E.; Gbureck, U. Passive and active in vitro resorption of calcium and magnesium phosphate cements by osteoclastic cells. *Tissue Eng. Part A* **2010**, *16*, 3687–3695. [[CrossRef](#)]
46. Sheikh, Z.; Zhang, Y.L.; Tamimi, F.; Barralet, J. Effect of processing conditions of dicalcium phosphate cements on graft resorption and bone formation. *Acta Biomater.* **2017**, *53*, 526–535. [[CrossRef](#)] [[PubMed](#)]
47. Bohner, M.; Theiss, F.; Apelt, D.; Hirsiger, W.; Houriet, R.; Rizzoli, G.; Gnos, E.; Frei, C.; Auer, J.; von Rechenberg, B. Compositional changes of a dicalcium phosphate dihydrate cement after implantation in sheep. *Biomaterials* **2003**, *24*, 3463–3474. [[CrossRef](#)]
48. Apelt, D.; Theiss, F.; El-Warrak, A.; Zlinszky, K.; Bettschart-Wolfisberger, R.; Bohner, M.; Matter, S.; Auer, J.; von Rechenberg, B. In vivo behavior of three different injectable hydraulic calcium phosphate cements. *Biomaterials* **2004**, *25*, 1439–1451. [[CrossRef](#)]
49. Grover, L.M.; Wright, A.J.; Gbureck, U.; Bolarinwa, A.; Song, J.; Liu, Y.; Farrar, D.F.; Howling, G.; Rose, J.; Barralet, J.E. The effect of amorphous pyrophosphate on calcium phosphate cement resorption and bone generation. *Biomaterials* **2013**, *34*, 6631–6637. [[CrossRef](#)]
50. Schröter, L.; Kaiser, F.; Stein, S.; Gbureck, U.; Ignatius, A. Biological and mechanical performance and degradation characteristics of calcium phosphate cements in large animals and humans. *Acta Biomater.* **2020**, *117*, 1–20. [[CrossRef](#)]
51. Kuemmerle, J.M.; Oberle, A.; Oechslin, C.; Bohner, M.; Frei, C.; Boeckel, I.; von Rechenberg, B. Assessment of the suitability of a new brushite calcium phosphate cement for cranioplasty—An experimental study in sheep. *J. Cranio-Maxillofac. Surg.* **2005**, *33*, 37–44. [[CrossRef](#)] [[PubMed](#)]

Disclaimer/Publisher’s Note: The statements, opinions and data contained in all publications are solely those of the individual author(s) and contributor(s) and not of MDPI and/or the editor(s). MDPI and/or the editor(s) disclaim responsibility for any injury to people or property resulting from any ideas, methods, instructions or products referred to in the content.